pK_a measurements for the SAMPL6 prediction challenge for a set of kinase inhibitor-like fragments

Mehtap Işık[1,2], **Dorothy Levorse**[3], **Ariën S. Rustenburg**[1,4], **Ikenna E. Ndukwe**[5], **Heather Wang**[6], **Xiao Wang**[5], **Mikhail Reibarkh**[5], **Gary E. Martin**[5], **Alexey A. Makarov**[6], **David L. Mobley**[7], **Timothy Rhodes**[3], **John D. Chodera**[1]*

[1]Computational and Systems Biology Program, Sloan Kettering Institute, Memorial Sloan Kettering Cancer Center, New York, NY 10065, United States; [2]Tri-Institutional PhD Program in Chemical Biology, Weill Cornell Graduate School of Medical Sciences, Cornell University, New York, NY 10065, United States; [3]Pharmaceutical Sciences, MRL, Merck & Co., Inc., 126 East Lincoln Avenue, Rahway, New Jersey 07065, United States; [4]Graduate Program in Physiology, Biophysics, and Systems Biology, Weill Cornell Medical College, New York, NY 10065, United States; [5]Process and Analytical Research and Development, Merck & Co., Inc., Rahway, NJ 07065, United States; [6]Analytical Research & Development, MRL, Merck & Co., Inc., MRL, 126 East Lincoln Avenue, Rahway, New Jersey 07065, United States; [7]Department of Pharmaceutical Sciences and Department of Chemistry, University of California, Irvine, Irvine, California 92697, United States

*For correspondence:
john.chodera@choderalab.org (JDC)

Abstract   Determining the net charge and protonation states populated by a small molecule in an environment of interest—such as solvent, a protein binding site, or a lipid bilayer—or the cost of altering those protonation states upon transfer to another environment is a prerequisite for predicting its physicochemical and pharmaceutical properties, as well as interactions with biological macromolecules using computational models. Incorrectly modeling the dominant protonation state, shifts in dominant protonation state, or the population of significant mixtures of protonation states can lead to large modeling errors that degrade the accuracy of physical modeling and hinder the ability to use physical modeling approaches for molecular design. For small molecules, the acid dissociation constant (pK_a) is the primary quantity needed to determine the ionic states populated by a molecule in an aqueous solution at a given pH. As a part of SAMPL6 community challenge, we organized a blind pK_a prediction component to assess the accuracy with which contemporary pK_a prediction methods can predict this quantity, with the ultimate aim of assessing the expected impact on modeling errors this would induce. While a multitude of approaches for predicting pK_a values currently exist, predicting the pK_as of drug-like molecules can be difficult due to challenging properties such as multiple titratable sites, heterocycles, and tautomerization. For this challenge, we focused on set of 24 small molecules selected to resemble selective kinase inhibitors—an important class of therapeutics replete with titratable moieties. Using a Sirius T3 instrument that performs automated acid-base titrations, we used UV absorbance-based pK_a measurements to construct a high-quality experimental reference dataset of macroscopic pK_as for the evaluation of computational pK_a prediction methodologies that was utilized in the SAMPL6 pK_a challenge. For several compounds in which the microscopic protonation states associated with macroscopic pK_as were ambiguous, we performed follow-up NMR experiments to disambiguate the microstates involved in the transition. This dataset provides a useful standard benchmark dataset for the evaluation of pK_a prediction methodologies on kinase inhibitor-like compounds.

42

Keywords

acid dissociation constants · spectrophotometric pK_a measurement · blind prediction challenge · SAMPL · macroscopic pK_a· microscopic pK_a· macroscopic protonation state · microscopic protonation state

Abbreviations

SAMPL Statistical Assessment of the Modeling of Proteins and Ligands

pK_a $-\log_{10}$ acid dissociation equilibrium constant

p$_s K_a$ $-\log_{10}$ apparent acid dissociation equilibrium constant in cosolvent

DMSO Dimethyl sulfoxide

ISA Ionic-strength adjusted

SEM Standard error of the mean

TFA Target factor analysis

LC-MS Liquid chromatography - mass spectrometry

NMR Nuclear magnetic resonance spectroscopy

HMBC Heteronuclear Multiple-Bond Correlation

TFA-*d* deutero-trifluoroacetic acid

Introduction

SAMPL (Statistical Assessment of the Modeling of Proteins and Ligands) is a recurring series of blind prediction challenges for the computational chemistry community [1, 2]. Through these challenges, SAMPL aims to evaluate and advance computational tools for rational drug design. By focusing the community on specific phenomena relevant to drug discovery poorly predicted by current models, isolating that phenomenon from other confounding factors in well-designed test systems, evaluating tools prospectively, enabling data sharing to learn from failures, and releasing the resulting high-quality datasets into the community as benchmark sets, SAMPL has driven progress in a number of areas over seven previous rounds of challenge cycles [3–7, 7–15].

As a stepping stone to enabling the accurate prediction of protein-ligand binding affinities, SAMPL has focused on evaluating how well physical and empirical modeling methodologies can predict various physicochemical properties relevant to binding and drug discovery, such as hydration free energies (which model aspects of desolvation in isolation), distribution coefficients (which model transfer from relatively homogeneous aqueous to nonpolar environments), and host-guest binding affinities (which model high-affinity association without the complication of slow protein dynamics). These physicochemical property prediction challenges—in addition to assessing the predictive accuracy of quantities that are useful in various stages of drug discovery in their own right—have been helpful in pinpointing deficiencies in computational models that can lead to substantial errors in affinity predictions.

Neglect of protonation state effects can lead to large modeling errors

As part of the SAMPL5 challenge series, a new cyclohexane-water distribution constant (log *D*) prediction challenge was introduced, where participants predicted the transfer free energy of small drug-like molecules between an aqueous buffer phase at pH 7.4 and a nonaqueous cyclohexane phase [16, 17]. While octanol-water distribution coefficient measurements are more common, cyclohexane was selected for the simplicity of its liquid phase and relative dryness compared to wet octanol phases. While the expectation was that this challenge would be relatively straightforward given the lack of complexity of cyclohexane phases, analysis of participant performance revealed that multiple factors contributed to significant prediction failures: poor conformational sampling of flexible solute molecules, misprediction of relevant protonation and tautomeric states (or failure to accommodate shifts in their populations), and force field inaccuracies resulting in bias towards the cyclohexane phase. While these findings justified the benefit of future iterations of blind distribution or partition coefficient challenges, the most surprising observation from this initial log *D* challenge was that participants almost uniformly neglected to accurately model protonation state effects,

89 and that neglect of these effects led to surprisingly large errors in transfer free energies [16–18]. Careful
90 quantum chemical assessments of the magnitude of these protonation state effects found that their neglect
91 could introduce errors up to 6–8 kcal/mol for some compounds [18]. This effect stems from the need to
92 account for the free energy difference between the major ionization state in cyclohexane (most likely neutral
93 state) and in water phase (which could be neutral or charged).

94 To isolate these surprisingly large protonation state modeling errors from difficulties related to lipophilic-
95 ity (log P and log D) prediction methods, we decided to organize a set of staged physicochemical property
96 challenges using a consistent set of molecules that resemble small molecule kinase inhibitors—an important
97 drug class replete with multiple titratable moieties. This series of challenges will first evaluate the ability
98 of current-generation modeling tools to predict acid dissociation constants (pK_a). It will be followed by a
99 partition/distribution coefficient challenge to evaluate the ability to incorporate experimentally-provided
100 pK_a values into prediction of distribution coefficients to ensure methodologies can correctly incorporate
101 protonation state effects into their predictions. A third challenge stage will follow: a new blinded parti-
102 tion/distribution coefficient challenge where participants must predict pK_a values on their own. At the
103 conclusion of this series of challenges, we will have ensured that modern physical and empirical modeling
104 methods have eliminated this large source of spurious errors from modeling both simple and complex
105 phenomena.

106 This article reports on the experiments for the first stage of this series of challenges: SAMPL6 pK_a
107 prediction challenge. The selection of a small molecule set and collection of experimental pK_a data are
108 described in detail.

Conceptualization of a blind pK_a challenge

110 This is the first time a blind pK_a prediction challenge has been fielded as part of SAMPL. In this first iteration of
111 the challenge, we aimed to assess the performance of current pK_a prediction methods and isolate potential
112 causes of inaccurate pK_a estimates.

113 The prediction of pK_a values for drug-like molecules can be complicated by several effects: the presence
114 of multiple (potentially coupled) titratable sites, the presence of heterocycles, tautomerization, the confor-
115 mational flexibility of large molecules, and ability of intramolecular hydrogen bonds to form. We decided
116 to focus on the chemical space of small molecule kinase inhibitors in the first iteration of pK_a prediction
117 challenge. A total of 24 small organic molecules (17 fragment-like and 7 drug-like) were selected for their
118 similarity to known small molecule kinase inhibitors, while also considering properties predicted to affect the
119 experimental tractability of pK_a and log P measurements such as solubility and predicted pK_as. Macroscopic
120 pK_a values were collected experimentally with UV-absorbance spectroscopy-based pK_a measurements using
121 a Sirius T3 instrument, which automates the sample handling, titration, and spectroscopic measurements
122 to allow high-quality pK_a determination. The Sirius T3 is equipped with an autosampler which allowed us
123 to run 8–10 measurements per day. Experimental data were kept blinded for three months (25 Oct 2017
124 through 23 Jan 2018) to allow participants in the SAMPL6 pK_a challenge to submit truly blinded computa-
125 tional predictions. Eleven research groups participated in this challenge, providing a total of 93 prediction
126 submission sets that cover a large variety of contemporary pK_a prediction methods.

Our selected experimental approach determines macroscopic pK_a values

128 Whenever experimental pK_a measurements are used for evaluating pK_a predictions, it is important to
129 differentiate between microscopic and macroscopic pK_a values. In molecules containing multiple titratable
130 moieties, the protonation state of one group can affect the proton dissociation propensity of another
131 functional group. In such cases, the **microscopic pK_a** (group pK_a) refers to the pK_a of deprotonation of
132 a single titratable group while all the other titratable and tautomerizable functional groups of the same
133 molecule are held fixed. Different protonation states and tautomer combinations constitute different
134 microstates. The **macroscopic pK_a** (molecular pK_a) defines the acid dissociation constant related to the
135 observable loss of a proton from a molecule regardless of which functional group the proton is dissociating
136 from, so it doesn't necessarily convey structural information.

137 Whether a measured pK_a is microscopic or macroscopic depends on the experimental method used
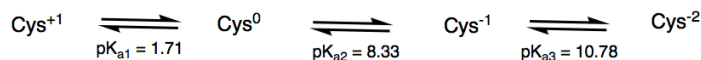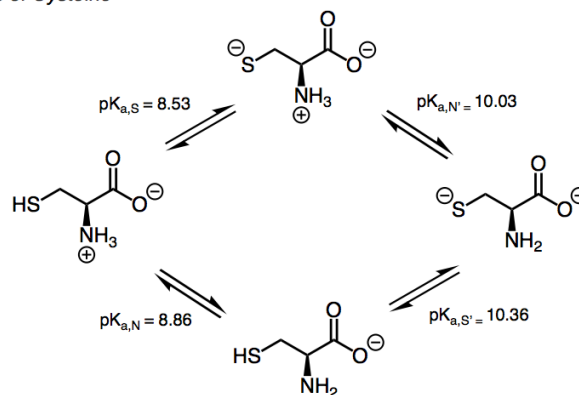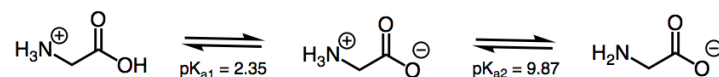
Macroscopic pK$_a$s of Cysteine

Cys^{+1} ⇌ Cys^0 ⇌ Cys^{-1} ⇌ Cys^{-2}
$pK_{a1} = 1.71$ $pK_{a2} = 8.33$ $pK_{a3} = 10.78$

Microscopic pK$_a$s of Cysteine

$pK_{a,S} = 8.53$ $pK_{a,N'} = 10.03$

$pK_{a,N} = 8.86$ $pK_{a,S'} = 10.36$

pK$_a$s of Glycine

$pK_{a1} = 2.35$ $pK_{a2} = 9.87$

Figure 1. Assignment of cysteine and glycine pK$_a$ values. pK_{a1}, pK_{a2}, and pK_{a3} are macroscopic acid dissociation constants for cysteine and glycine [24]. When pK$_a$ values of a polyprotic molecule are very different, such as in the case of glycine, it is possible to assign the pK$_a$s to individual groups since the dissociation of protons is stepwise [19]. However, stepwise dissociation can not be assumed for cysteine, because pK_{a2} and pK_{a3} are very close in value. Four underlying microscopic pK$_a$s ($pK_{a,S}$, $pK_{a,N}$, $pK_{a,S'}$, and $pK_{a,N'}$) for cysteine were measured using UV spectra analysis of cysteine and derivatives [25]. Notice that the proximity of $pK_{a,S}$ and $pK_{a,N}$ values indicates similar probability of proton dissociation from these groups. This figure is adopted from [19].

138   (Figure 2). For a molecule with only one titratable proton, the microscopic pK$_a$ is equal to the macroscopic
139   pK$_a$. For a molecule with multiple titratable groups, however, throughout a titration from acidic to basic pH,
140   the deprotonation of some functional groups can take place almost simultaneously. For these multiprotic
141   molecules, the experimentally-measured macroscopic pK$_a$ will include contributions from multiple micro-
142   scopic pK$_a$s with similar values (i.e., acid dissociation of multiple microstates). Cysteine provides an example
143   of this behavior with its two macroscopic pK$_a$s observable by spectrophotometric or potentiometric pK$_a$
144   measurement experiments [19, 20].

145   While four microscopic pK$_a$s can be defined for cysteine, experimentally observed pK$_a$ values can't be
146   assigned to individual functional groups directly (Figure 1, *top*), and more advanced techniques capable of
147   resolving individual protonation sites—such as NMR [21], Raman spectroscopy [22, 23], and the analysis of
148   pK$_a$s in molecular fragments or derivatives—are required to unambiguously assign the site of protonation
149   state changes. On the other hand, when there is a large difference between microscopic pK$_a$s in a multiprotic
150   molecule, the proton dissociations won't overlap and macroscopic pK$_a$s observed by experiments can be
151   assigned to individual titratable groups. The pK$_a$ values of glycine provide a good example of this scenario
152   (Figure 1, *bottom*) [19, 20, 22]. We recommend the short review on the assignment of pK$_a$values authored by
153   Ivan G. Darvey [20] for a good introduction to the concepts of macroscopic *vs* microscopic pK$_a$ values.

154   The most common methods for measuring small molecule pK$_a$s are UV-absorbance spectroscopy (UV-
155   metric titration) [28–30], potentiometry (pH-metric titration) [30, 31], capillary electrophoresis [32, 33],
156   and NMR spectroscopy [21], with NMR being the most time-consuming approach. Other, less popular pK$_a$
157   measurement techniques include conductometry, HPLC, solubility or partition based estimations, calorimetry,
158   fluorometry, and polarimetry [34]. UV-metric and pH-metric methods (Figure 3) are limited to measuring
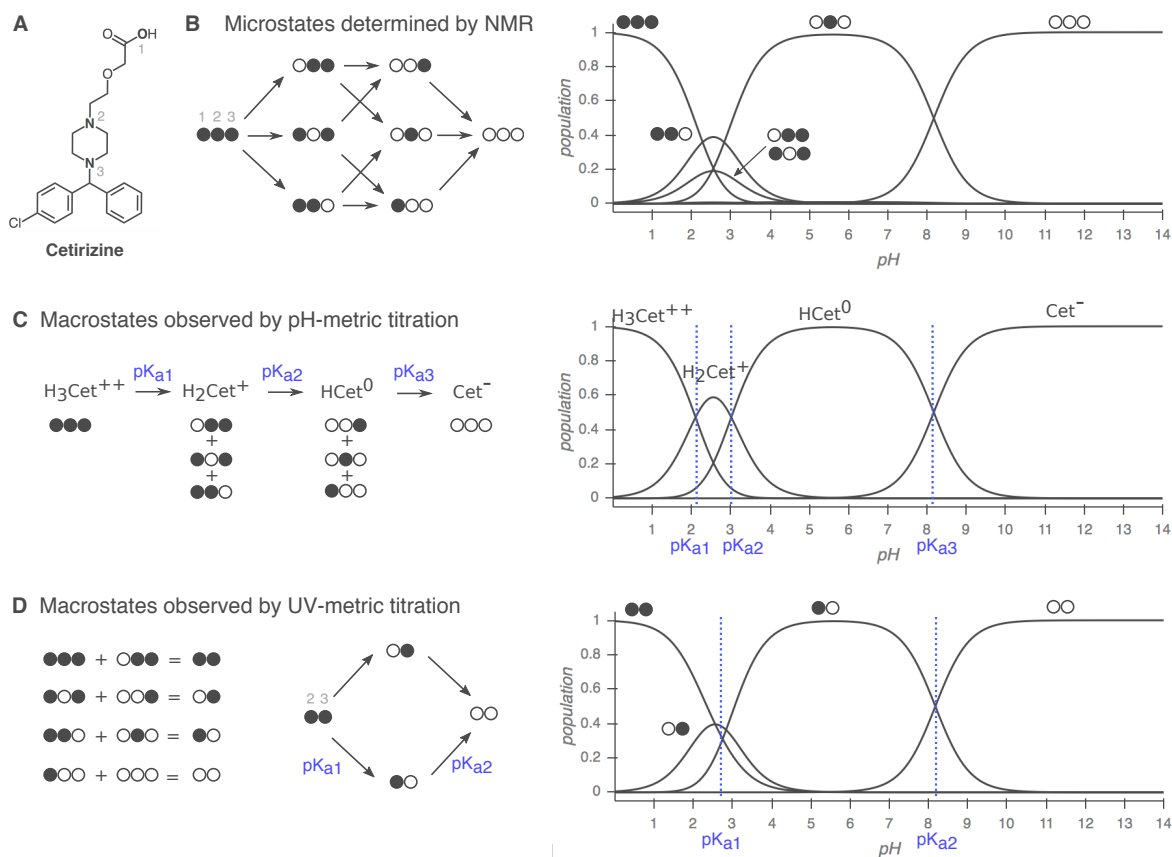
Figure 2. Comparison of macroscopic and microscopic pK_a measurement methods. Filled circles represent protonated sites and empty circles represent deprotonated sites with the order of carboxylic acid (1), piperazine nitrogen (2), and piperazine nitrogen (3). Protonation state populations shown for pH-metric and UV-metric pK_a measurement methods are simulations, calculated using NMR-based microscopic pK_a values. (**A**) Cetirizine has $n = 3$ titratable sites, shown in bold. (**B**) *Left:* The 8 microstates (2^n) and 12 microscopic pK_as ($n2^{n-1}$) of cetirizine. *Right:* Relative population of microspecies with respect to pH. Potentially all microstates can be resolved via NMR. (**C**) Simulated pH-metric (potentiometric) titration and macroscopic populations. For a polyprotic molecule, only macroscopic pK_as can be measured with pH-metric titration. Microstates with different total charge (related to the number of protons) can be resolved, but microstates with the same total charge are observed as one macroscopic population. (**D**) Simulated microscopic populations for UV-metric (spectrophotometric) titration of cetirizine. Since only protonation of the titration sites within four heavy atoms of the UV-chromophore is likely to cause an observable change in the UV-absorbance spectra, microstates that only differ by protonation of the distal carboxylic acid cannot be differentiated. Moreover, populations that overlap may or may not be resolvable depending on how much their absorbance spectra in the UV region differ. Both UV-metric and pH-metric pK_a determination methods measure macroscopic pK_as for polyprotic molecules, which cannot easily be assigned to individual titration sites and underlying microstate populations in the absence of other experimental evidence that provides structural resolution, such as NMR. Note that macroscopic populations observed in these two methods are composed of different combinations of microstates depending on the principles of measurement technique. Here, the illustrative diagram style was adopted from [26], and NMR-determined microscopic pK_as for cetirizine were taken from [27].

159 aqueous pK_a values between 2 and 12 due to limitations of the pH electrode used in these measurements.
160 The pH-metric method relies on determining the stoichiometry of bound protons with respect to pH,
161 calculated from volumetric titration with acid or base solutions. Accurate pH-metric measurements require
162 high concentrations of analyte as well as analytically prepared acid/base stocks and analyte solutions.
163 By contrast, UV-metric pK_a measurements rely on the differences in UV absorbance spectra of different
164 protonation states, generally permitting lower concentrations of analyte to be used. The pH and UV
165 absorbance of the analyte solution are monitored during titration.

166 Both UV-metric and pH-metric pK_a determination methods measure macroscopic pK_as for polyprotic
167 molecules, which can not be easily assigned to individual titration sites and underlying microstate popu-
168 lations in the absence of other experimental evidence that provides structural information, such as NMR
169 (Figure 2). Macroscopic populations observed in these two methods are composed of different combinations
170 of microstates depending on the principles of measurement technique. In potentiometric titrations, mi-
171 crostates with same total charge will be observed as one macrostate, while in spectrophotometric titrations,
172 protonation sites remote from chromophores might be spectroscopically invisible, and macrostates will be
173 formed from collections of microstates that manifest similar UV-absorbance spectra.

174 Spectrophotometric pK_a determination is more sensitive than potentiometric determination, requiring
175 low analyte concentrations (50–100 μM)—especially advantageous for compounds with low solubilities—
176 but is only applicable to titration sites near chromophores. For protonation state changes to affect UV
177 absorbance, a useful rule of thumb is that the protonation site should be a maximum of four heavy atoms
178 away from the chromophore, which might consist of conjugated double bonds, carbonyl groups, aromatic
179 rings, etc. Although potentiometric measurements do not suffer from the same observability limitations,
180 higher analyte concentrations (∼5 mM) are necessary for the analyte to provide sufficiently large enough
181 buffering capacity signal above water to produce an accurate measurement. The accuracy of pK_as fit to
182 potentiometric titrations can also be also sensitive to errors in the estimated concentration of the analyte in
183 the sample solution, while UV-metric titrations are insensitive to concentration errors. We therefore decided
184 to adopt spectrophotometric measurements for collecting the experimental pK_a data for this challenge, and
185 selected a compound set to ensure that all potential titration sites are in the vicinity of UV chromophores.

186 Here, we report on the selection of SAMPL6 pK_a challenge compounds, their macroscopic pK_a values
187 measured by UV-metric titrations using a Sirius T3, as well as NMR-based microstate characterization of two
188 SAMPL6 compounds with ambiguous protonation states associated with the observed macroscopic pK_as
189 (SM07 and SM14). We discuss implications of the use of this experimental technique for the interpretation
190 of pK_a data, and provide suggestions for future pK_a data collection efforts with the goal of evaluating or
191 training computational pK_a predictions.

Methods

Compound selection and procurement

194 To select a set of small molecules focusing on the chemical space representative of kinase inhibitors for
195 physicochemical property prediction challenges (pK_a and lipophilicity) we started from the kinase-targeted
196 subclass of the ZINC15 chemical library [35] and applied a series of filtering and selection rules as depicted
197 in Figure 4A. We focused on the availability "now" and reactivity "anodyne" subsets of ZINC15 in the first
198 filtering step [http://zinc15.docking.org/subclasses/kinase/substances/subsets/now+anodyne/]. The "now"
199 label indicates the compounds were availabile for immediate delivery, while the "anodyne" label excludes
200 compounds matching filters that flag compounds with the potential for reactivity or pan-assay interference
201 (PAINs) [36, 37].

202 Next, we identified resulting molecules that were also available for procurement through eMolecules [38]
203 (free version, downloaded 1 June 2017), the supplier that would be used for procurement in this exercise. To
204 find the intersection of ZINC15 kinase subset and eMolecules database, we matched molecules using their
205 canonical isomeric SMILES strings, as computed via the OpenEye OEChem Toolkit (version 2017.Feb.1) [39].

206 To extract availability and price information from eMolecules, we queried using a list of SMILES (as
207 reported in eMolecules database) of the intersection set. We further filtered the intersection set (1204
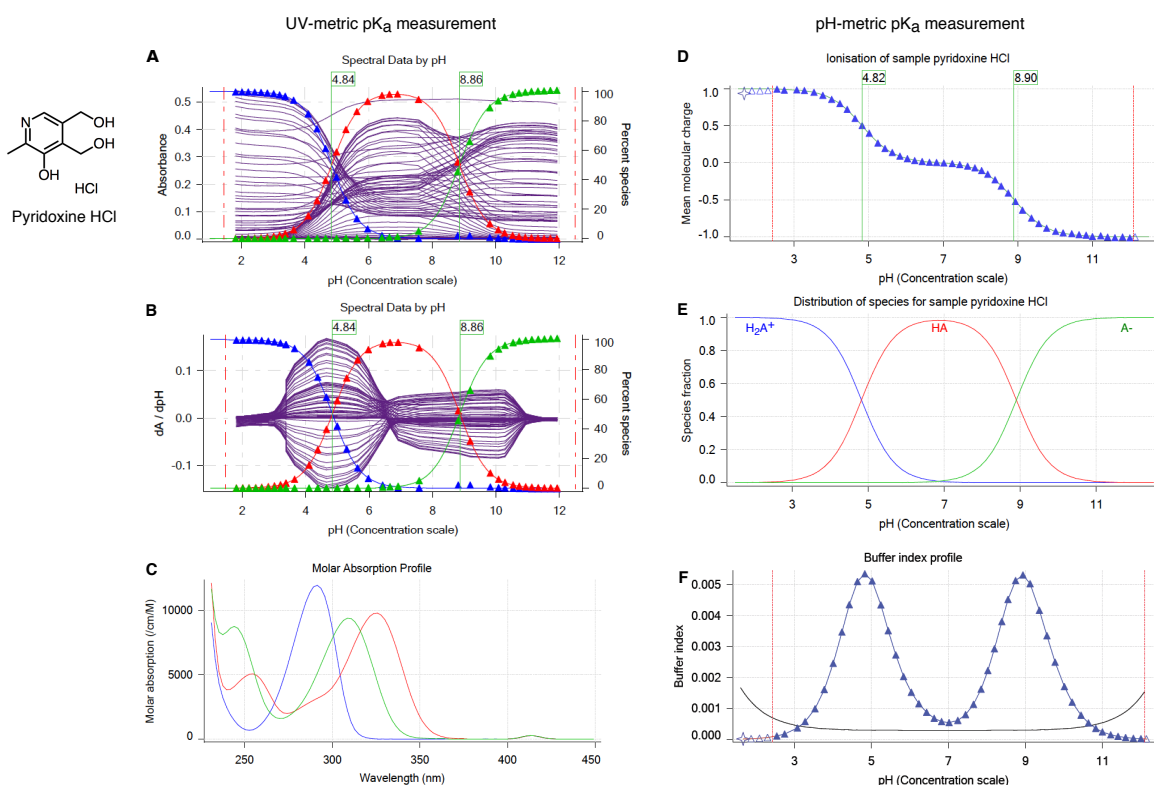
Figure 3. UV-metric (spectrophotometric) and pH-metric (potentiometric) pK_a measurements of pyridoxine HCl with Sirius T3. Spectrophotometic pK_a measurement (panels **A, B, C**) relies on differences in the UV absorbance spectra between microscopic protonation states to deconvolute the population of macrostate species as a function of pH. While highly sensitive (and therefore requiring a very low analyte concentration of ~ 50 μM), this approach can only resolve changes in protonation states for titratable sites near chromophores and cannot separate the populations of microstates that change in the same manner as a function of pH. (**A**) Multiwavelength UV absorbance vs pH. Purple lines represents absorbance at distinct wavelengths in UV region. (**B**) Derivative of multiwavelength absorbance with respect to pH (dA/dpH) vs pH is plotted with purple lines. In **A** and **B**, blue, red, and green triangles represent population of protonation states (from most protonated to least protonated) as calculated from a global fit to experimental UV absorbances for all pH values, while thin lines denote model fits that utilize the fitted model pK_as to compute populations. pK_a values (green flags) correspond to inflection point of multiwavelength absorbance data where change in absorbance with respect to pH is maximum. (**C**) Molar absorption coefficients vs wavelength for each protonation state as resolved by TFA. **D, E, F** illustrate potentiometric pK_a measurement where molar addition of acid or base is tracked as pH is titrated. (**D**) Mean molecular charge vs pH. Mean molecular charge is calculated based on the model provided for the analyte: predicted number and nature of titratable sites (acid or base type), and number of counter ions present. pK_a values are calculated as inflection points of charge vs pH plot. (**E**) Predicted macroscopic protonation state populations vs pH calculated based on pK_a values (H$_2$A$^+$: blue, HA: red, and A$^-$: green) (**F**) Buffering index vs pH profile of water (grey solid line, theoretical) and the sample solution (blue triangles represent experimental data points). A higher concentration of analyte (~5 mM) is necessary for the potentiometric method than the spectrophotometric method in order to provide large enough buffering capacity signal above water for an accurate measurement.

208 compounds) based on delivery time (Tier 1 suppliers, two-week delivery) and at least 100 mg availability in
209 powder form (format: Supplier Standard Vial). We aimed to purchase 100 mg of each compound in powder
210 form with at least 90% purity. We calculated 100 mg was enough for optimization and replicate experiments
211 to measure pK_a, log P, and solubility measurements with the Sirius T3. Each UV-metric and pH-metric pK_a
212 measurement requires a minimum of 0.01 mg and 1.00 mg compound (solid or delivered via DMSO stock
213 solution), respectively. logP and pH-dependent solubility measurements require around 2 mg and 10 mg of
214 solid chemical, respectively.

Filtering for predicted measurable pK_as and lack of experimental data

216 The Sirius T3 (Pion) instrument used to collect pK_a and log P/log D measurements requires a titratable group
217 in the pK_a range of 2–12, so we aimed to select compounds with predicted pK_as in the range of 3–11 to allow a
218 ~1 pK unit margin of error in pK_a predictions. pK_a predictions for compound selection were calculated using
219 Epik (Schödinger) sequential pK_a prediction (scan) [40, 41] with target pH 7.0 and tautomerization allowed
220 for generated states. We filtered out all compounds that did not have any predicted pK_as between 3–11, as
221 well as compounds with two pK_a values predicted to be less than 1 pK_a unit apart in the hopes that individual
222 pK_as of multiprotic compounds could be resolved with spectrophotometric pK_a measurements. With the
223 goal of selecting compounds suitable for subsequent log P measurements, we eliminated compounds
224 with OpenEye XlogP [42] values less than -1 or greater than 6. Subsets of compounds with molecular
225 weights between 150–350 g/mol and 350–500 g/mol were selected for fragment-like and drug-like categories
226 respectively. Compounds without available price or stock quantity information were eliminated. As the goal
227 was to provide a blind challenge, compounds with publicly available experimental log P measurements were
228 also removed. The sources we checked for publicly available experimental log P values were the following:
229 DrugBank [43] (queried with eMolecules SMILES), ChemSpider [44] (queried by canonical isomeric SMILES),
230 NCI Open Database August 2006 release [45], Enhanced NCI Database Browser [46] (queried with canonical
231 isomeric SMILES), and PubChem [47] (queried with InChIKeys generated from canonical isomeric SMILES
232 with NCI CACTUS Chemical Identifier Resolver [48]).

Filtering for kinase inhibitor-like scaffolds

234 In order to include common scaffolds found in kinase inhibitors, we analyzed the frequency of rings
235 found in FDA-approved kinase inhibitors via Bemis-Murcko fragmentation using OEMedChem Toolkit of
236 OpenEye [49, 50]. Heterocycles found more than once in FDA-approved kinase inhibitors are shown in
237 Figure 4B. In selecting 25 compounds for the fragment-like set and 10 compounds for the drug-like set, we
238 prioritized including at least one example of each heterocycle, although we failed to find compounds with
239 piperazine and indazole that satisfied all other selection criteria. We observed that certain heterocycles
240 (shown in Figure 4C) were overrepresented based on our selection criteria; therefore, we limited the number
241 of these structures in the SAMPL6 challenge set to at most one in each set. To achieve broad and uniform
242 sampling of the measurable log P dynamic range, we segregated the molecules into bins of predicted XlogP
243 values and selected compounds from each bin, prioritizing less expensive compounds.

Filtering for UV chromophores

245 The presence of UV chromophores (absorbing in the 200–400 nm range) in close proximity to protonation
246 sites is necessary for spectrophotometric pK_a measurements. To filter for molecules with UV chromophores,
247 we looked at the substructure matches to the SMARTS pattern `[n,o,c][c,n,o]cc` which was considered
248 the smallest unit of pi-conjugation that can constitute a UV chromophore. This SMARTS pattern describes
249 extended conjugation systems comprised of four heavy atoms and composed of aromatic carbon, nitrogen,
250 or oxygen, such as 1.3-butadiene, which possesses an absorption peak at 217 nm. Additionally, the final set
251 of selected molecules was manually inspected to makes sure all potentially titratable groups were no more
252 than four heavy atoms away from a UV chromophore.

253 25 fragment-like and 10 drug-like compounds were selected, out of which procurement of 28 was
254 completed in time. pK_a measurements for 17 (SM01–SM17) and 7 (SM18–SM24) were successful, respectively.
255 The resulting set of 24 small molecules constitute the SAMPL6 pK_a challenge set. For the other four
256 compounds, UV-metric pK_a measurements show no detectable pK_as in the range of 2–12, so we decided not

257 to include them in the SAMPL6 pK_a challenge. Experiments for these four compounds are not reported in
258 this publication.

259 Python scripts used in the compound selection process are available from GitHub [https://github.com/
260 choderalab/sampl6-physicochemical-properties]. Procurement details for each compound can be found
261 in Supplementary Table 1. Chemical properties used in the selection of compounds are summarized in
262 Supplementary Table 2.

UV-metric pK_a measurements

264 Experimental pK_a measurements were collected using the spectrophotometric pK_a measurement method
265 with a Sirius T3 automated titrator instrument (Pion) at 25°C and constant ionic strength. The Sirius T3
266 is equipped with an Ag/AgCl double-junction reference electrode to monitor pH, a dip probe attached to
267 UV spectrophotometer, a stirrer, and automated volumetric titration capability. The Sirius T3 UV-metric
268 pK_a measurement protocol measures the change in multi-wavelength absorbance in the UV region of the
269 absorbance spectrum while the pH is titrated over pH 1.8–12.2 [28, 29]. UV absorbance data is collected
270 from 160–760 nm while the 250–450 nm region is typically used for pK_a determinations. Subsequent global
271 data analysis identifies pH-dependent populations of macrostates and fits one or more pK_a values to match
272 this population with a pH-dependent model.

273 DMSO stock solutions of each compound with 10 mg/ml concentration were prepared by weighing 1 mg
274 of powder chemical with a Sartorius Analytical Balance (Model: ME235P) and dissolving it in 100 μL DMSO
275 (Dimethyl sulfoxide, Fisher Bioreagents, CAT: BP231-100, LOT: 116070, purity ≥ 99.7%). DMSO stock solutions
276 were capped immediately to limit water absorption from the atmosphere due to the high hygroscopicity
277 of DMSO and sonicated for 5–10 minutes in a water bath sonicator at room temperature to ensure proper
278 dissolution. These DMSO stock solutions were stored in room temperature up to two weeks in capped glass
279 vials. 10 mg/ml DMSO solutions were used as stock solutions for the preparation of three replicate samples
280 for the independent titrations. For each experiment, 1–5 μL of 10 mg/ml DMSO stock solution was delivered
281 to a 4 mL Sirius T3 glass sample vial with an electronic micropipette (Rainin EDP3 LTS 1–10 μL). The volume
282 of delivered DMSO stock solution, which determines the sample concentration following dilution by the
283 Sirius T3, is optimized individually for each compound to achieve sufficient but not saturated absorbance
284 signal (targeting 0.5–1.0 AU) in the linear response region. Another limiting factor for sample concentration
285 was ensuring that the compound remains soluble throughout the entire pH titration range. An aliquot of
286 25 μL of mid-range buffer (14.7 mM K_2HPO_4 and 0.15 M KCl in H_2O) was added to each sample, transferred
287 with a micropipette (Rainin EDP3 LTS 10–100 μL) to provide enough buffering capacity in middle pH ranges
288 so that pH could be controlled incrementally throughout the titration.

289 pH is temperature and ionic-strength dependent. A peltier device on the Sirius T3 kept the analyte
290 solution at 25.0 ± 0.5 °C throughout the titration. Sample ionic strength was adjusted by dilution in 1.5 mL
291 ionic strength-adjusted water (ISA water ≡ 0.15 M KCl in H_2O) by the Sirius T3. Analyte dilution, mixing,
292 acid/base titration, and measurement of UV absorbance was automated by the Sirius T3 UV-metric pK_a
293 measurement protocol. The pH was titrated between pH 1.8 and 12.2 via the addition of acid (0.5 M HCl)
294 and base (0.5 M KOH), targeting 0.2 pH steps between UV absorbance spectrum measurements. Titrations
295 were performed under argon flow on the surface of the sample solution to limit the absorption of carbon
296 dioxide from air, which can alter the sample pH to a measurable degree. To fully capture all sources of
297 experimental variability, instead of performing three sequential pH titrations in the same sample solution,
298 three replicate samples (prepared from the same DMSO stock solution) were subjected to one round of
299 pH titration each. Although this choice reduced throughput and increased analyte consumption, it limited
300 the dilution of the analyte during multiple titrations, resulting in stronger absorbance signal for pK_a fitting.
301 Under circumstances where analyte is scarce, it is also possible to do three sequential titrations using the
302 same sample to limit consumption when the loss of accuracy is acceptable.

303 Visual inspection of the sample solutions after titration and inspection of the pH-dependent absorbance
304 shift in the 500–600 nm region of the UV spectra was used to verify no detectable precipitation occurred
305 during the course of the measurement. Increased absorbance in the 500–600 nm region of the UV spectra is
306 associated with scattering of longer wavelengths of light in the presence of colloidal aggregates. For each
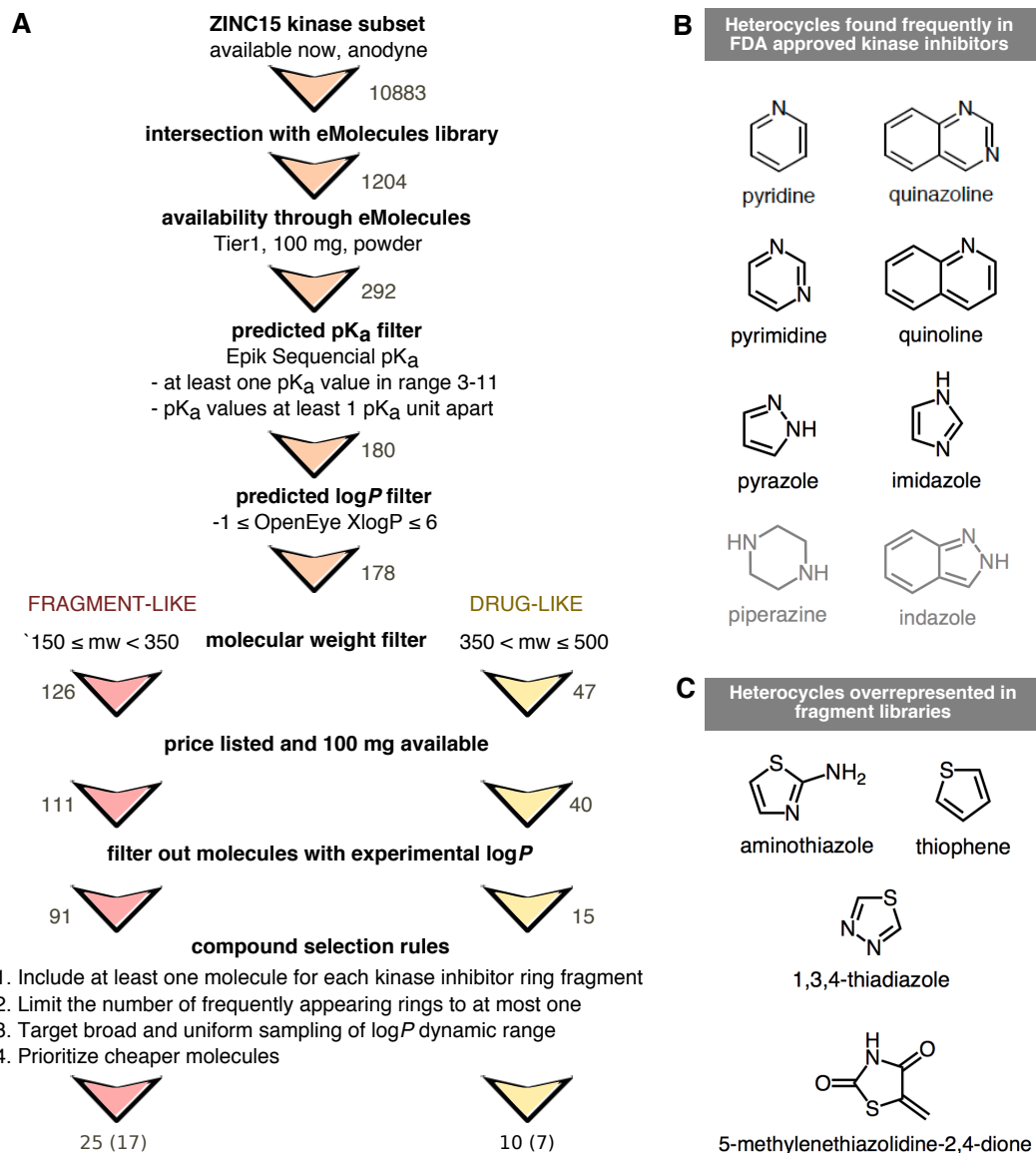
Figure 4. Compound selection for the SAMPL6 pK_a challenge, with the goal of running subsequent log P/log D challenges on the same compound set. (**A**) Flowchart of filtering steps for the selection of compounds that resemble kinase inhibitors and their fragments. Numbers next to arrows indicate the number of compounds remaining after each filtering step. A total of 25 fragment-like and 10 drug-like compounds were selected, out of which procurement and pK_a measurements for 17 fragment-like and 7 drug-like compounds were successful, respectively. (**B**) Frequent heterocycles found in FDA approved kinase inhibitors, as determined by Bemis-Murcko fragmentation into rings [49]. Black structures were represented in SAMPL6 set at least once. Compounds with piperazine and indazole (gray structures) could not be included in the challenge set due to library and selection limitations. (**C**) Structures of heterocycles that were overrepresented based on our compound selection workflow. We have limited the number of occurrences of these heterocycles to at most one.

307 analyte, we optimized analyte concentration, direction of the titration, and pH titration range in order to
308 maintain solubility over the entire experiment. The titration direction was specified so that each titration
309 would start from the pH where the compound is most soluble: low-to-high pH for bases and high-to-low
310 pH for acids. While UV-metric pK_a measurements can be performed with analyte concentrations as low as
311 50 µM (although this depends on the absorbance properties of the analyte), some compounds may yet not
312 be soluble at these low concentrations throughout the pH range of the titration. As the sample is titrated
313 through a wide range of pH values, it is likely that low-solubility ionization states—such as neutral and
314 zwitterionic states—will also be populated, limiting the highest analyte concentration that can be titrated
315 without encountering solubility issues. For compounds with insufficient solubility to accurately determine a
316 pK_a value directly in a UV-metric titration, a cosolvent protocol was used, as described in the next section
317 (**UV-metric pK_a measurement with cosolvent**).

318   Two Sirius T3 computer programs—Sirius T3 Control v1.1.3.0 and Sirius T3 Refine v1.1.3.0—were used
319 to execute measurement protocols and analyze pH-dependent multivelenghth spectra, respectively. Pro-
320 tonation state changes at titratable sites near chromophores will modulate the UV-absorbance spectra of
321 these chromophores, allowing populations of distinct UV-active species to be resolved as a function of pH.
322 To do this, basis spectra are identified and populations extracted via TFA analysis of the pH-dependent
323 multi-wavelength absorbance [29]. When fitting the absorbance data to a titratable molecule model to
324 estimate pK_as, we selected the minimum number of pK_as sufficient to provide a high-quality fit between
325 experimental and modeled data based on visual inspection of pH-dependent populations.

326   This method is capable of measuring pK_a values between 2–12 when titratable groups are at most 4–5
327 heavy atoms away from chromophores such that a change in protonation state alters the absorbance
328 spectrum of the chromophore. We selected compounds where titratable groups are close to potential
329 chromophores (generally aromatic ring systems), but the possibility exists that our experiments did not
330 detect protonation state changes of titratable groups distal from UV chromophores.

Cosolvent UV-metric pK_a measurements of molecules with poor aqueous solubilities

332 If analytes are not sufficiently soluble during the titration, pK_a values cannot be accurately determined via
333 aqueous titration directly. If precipitation occurs, the UV-absorbance signal from pH-dependent precipitate
334 formation can not be differentiated from the pH-dependent signal of soluble microstate species. For com-
335 pounds with low aqueous solubility, pK_a values were estimated from multiple apparent pK_a measurements
336 performed in ISA methanol:ISA water cosolvent solutions with various mole fractions, from which the pK_a
337 at 0% methanol (100% ISA water) can be extrapolated. This method is referred to as a UV-metric p$_s K_a$
338 measurement in the Sirius T3 Manual [51].

339   The cosolvent spectrophotometric pK_a measurement protocol was very similar to the standard aqueous
340 UV-metric pK_a measurement protocol, with the following differences: titrations were performed in typically
341 in 30%, 40%, and 50% mixtures of ISA methanol:ISA water by volume to measure apparent pK_a values (p$_s K_a$)
342 in these mixtures. Yasuda-Shedlovsky extrapolation was subsequently used to estimate the pK_a value at 0%
343 cosolvent (Figure 5) [31, 52, 53].

$$p_s K_a + \log[H_2O] = A/\epsilon + B \tag{1}$$

344 Yasuda-Shedlovsky extrapolation relies on the linear correlation between p$_s K_a + \log[H_2O]$ and the reciprocal
345 dielectric constant of the cosolvent mixture ($1/\epsilon$). In Eq. 1, A and B are the slope and intercept of the line
346 fitted to experimental datapoints. Depending on the solubility requirements of the analyte, the methanol
347 ratio of the cosolvent mixtures was adjusted. We designed the experiments to have at least 5% cosolvent
348 ratio difference between datapoints and no more than 60% methanol content. Calculation of the Yasuda-
349 Shedlovsky extrapolation was performed by the Sirius T3 software using at least 3 p$_s K_a$ values measured in
350 different ratios of methanol:water. Addition of methanol (80%, 0.15 M KCl) was controlled by the instrument
351 before each titration. Three consecutive pH titrations at different methanol concentrations were performed
352 using the same sample solution. In addition, three replicate measurements with independent samples
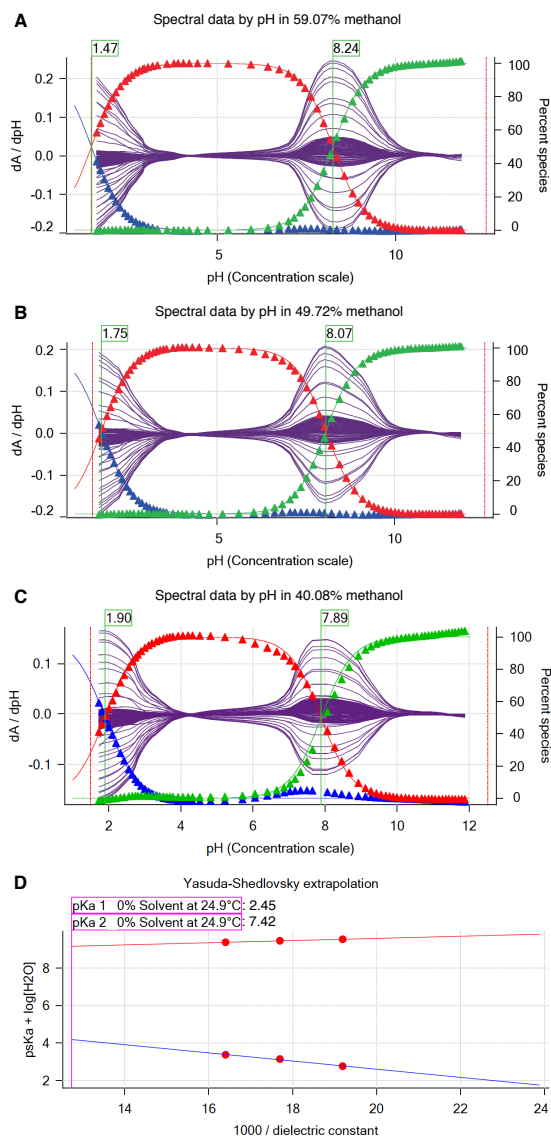353 (prepared from the same DMSO stock) were collected.

Figure 5. Determination of SM22 pK_a values with cosolvent method and Yasuda-Shedlovsky extrapolation. A, **B**, and **C** show p_sK_a of SM22 determined at various methanol concentrations: 59.07%, 49.72%, 40.08% by weight. Purple solid lines indicate the derivative of the absorbance signal with respect to pH *vs* pH at multiple wavelengths. p_sK_a values (green flags) were determined by Sirius T3 Refine Software. Blue, red, and green triangles show relative populations of macroscopic protonation states with respect to pH calculated from the experimental data. Notice that as cosolvent concentration increases, p_sK_{a1} decreases from 1.90 to 1.47 and p_sK_{a2} increases from 7.84 to 8.24. **D** Yasuda-Shedlovsky extrapolation plot for SM22. Red datapoints correspond to p_sK_a determined at various cosolvent ratios. Based on linear fitting to $p_sK_a + log[\mathrm{H_2O}]$ vs $1/\epsilon$, pK_{a1} and pK_{a2} in 0% cosolvent (aqueous solution) was determined as 2.45 and 7.42, respectively. R^2 values of linear fits are both 0.99. The slope of Yasuda-Shedlovsky extrapolation shows if the observed titration has acidic (positive slope) or basic (negative slope) character dominantly, although this is an macroscopic observation and should not be relied on for annotation of pK_as to functional groups (microscopic pK_as).

Calculation of uncertainty in pK_a measurements

Experimental uncertainties were reported as the standard error of the mean (SEM) of three replicate pK_a measurements. The standard error of the mean (SEM) was estimated as

$$\text{SEM} = \frac{\sigma}{\sqrt{N}} \quad ; \quad \sigma = \sqrt{\frac{1}{N}\sum_{i=1}^{N}(x_i - \mu)^2} \quad ; \quad \mu = \frac{1}{N}\sum_{i=1}^{N} x_i \tag{2}$$

where σ denotes the sample standard deviation and μ denotes the sample mean. x_i are observations and N is the number of observations.

Since the Sirius T3 software reports pK_a values to only two decimal places, we have reported the SEM as 0.01 in cases where SEM values calculated from 3 replicates were lower than 0.01. SEM calculated from replicate measurements were found to be larger than non-linear fit error reported by the Sirius T3 Refine Software from UV-absorbance model fit of a single experiment, thus leading us to believe that running replicate measurements and reporting mean and SEM of pK_a measurements is better for capturing all sources of experimental uncertainty. Notably, for UV-metric measurements, the measured pK_a values should be insensitive to final analyte concentration and any uncertainty in the exact analyte concentration of the original DMSO stock solution, justifying the use of the same stock solution (rather than independently prepared stock solutions) for multiple replicates.

Quality control for chemicals

Compound purity was assessed by LC-MS using an Agilent HPLC 1200 Series equipped with auto-sampler, UV diode array detector, and a Quadrupole MS detector 6140. ChemStation version C01.07SR2 was used to analyze LC & LC/MS. An Ascentis Express C18 column (3.0 x 100 mm, 2.7 μm) was used, with column temperature set at 45° C.

- Mobile phase A: 2 mM ammonium formate (pH = 3.5) aqueous
- Mobile phase B: 2 mM ammonium formate in 90:10 acetonitrile:water (pH = 3.5)
- Flow rate : 0.75 ml/min
- Gradient: Starting with 10% B to 95% B in 10 minutes then hold at 95% B for 5 minutes.
- Post run length: 5 minutes
- Mass condition: ESI positive and negative mode
- Capillary voltage: 3000 V
- Drying gas flow: 12 ml/min
- Nebulizer pressure: 35 psi
- Drying temperature: 350°C
- Mass range: 5-1350 Da; Fragmentor: 70; Threshold: 100

The percent area for the primary peak is calculated based on the area of the peak divided by the total area of all peaks. The percent area of the primary peak is reported as an estimate of sample purity. The purity of primary LC peak was checked by ChemStation software with threshold 995, to check that there is no significant impurity underneath the main peak.

NMR determination of protonation microstates

In general, the chemical shifts of nuclear species observed in nuclear magnetic resonance (NMR) spectra report on and are very sensitive to the chemical environment. Consequently, small changes in chemical environment, such as the protonation events described in this work, are manifest as changes in the chemical shift(s) of the nuclei. If perturbation occurs at a rate which is fast on the NMR timescale (*fast exchange*), an average chemical shift is observed. This phenomena has been exploited and utilized as a probe for determining the order of protonation for molecules with more than one titratable site [54]. In some cases, direct observation of the titrated nuclei can be difficult, for example nitrogen and oxygen, due to sample limitations and/or low natural abundance of the NMR active nuclei (0.37% for ^{15}N and 0.038% for ^{17}O)—amongst other factors. In these situations, chemical shifts changes of the so-called "reporter" NMR

398 nuclei—^{1}H, ^{31}P, or ^{13}C nuclei, which are directly attached to or are a few bonds away from the titrated
399 nuclei—have been utilized as the probe for NMR-pH titrations [21, 55, 56]. This approach is advantageous
400 since the sensitive NMR nuclides (^{1}H and ^{31}P) are observed. In addition, ^{31}P and ^{13}C offer large spectral
401 widths of ~300 ppm and ~200 ppm, respectively, which minimize peak overlap.

402 However, reporter nuclei chemical shifts provide indirect information subject to interpretation. In complex
403 systems with multiple titratable groups, such analysis will be complicated due to a cumulative effect of these
404 groups on the reporter nuclide due to their close proximity or the resonance observed in aromatic systems.
405 In contrast, direct observation of the titratable nuclide where possible, affords a more straight-forward
406 approach to studying the protonation events. In this study, the chemical shifts of the titratable nitrogen
407 nuclei were observed using the ^{1}H-^{15}N-HMBC (Heteronuclear Multiple-Bond Correlation) experiments — a
408 method that affords the observation of ^{15}N chemical shifts while leveraging the sensitivity accrued from the
409 high abundance the ^{1}H nuclide.

410 The structures of samples SM07 and SM14 were assigned via a suite of NMR experiments, which included
411 ^{1}H NMR, ^{13}C NMR, homonuclear correlated spectroscopy (^{1}H-^{1}H COSY), heteronuclear single quantum
412 coherence (^{1}H-^{13}C HSQC), ^{13}C heteronuclear multiple-bond correlation (^{1}H-^{13}C-HMBC) and ^{15}N heteronuclear
413 multiple-bond correlation (^{1}H-^{15}N-HMBC)—see SI. All NMR data used in this analysis were acquired on a
414 Bruker 500 MHz spectrometer equipped with a 5 mm TCI CryoProbe^{TM} Prodigy at 298 K. The poor solubility
415 of the analytes prevented analysis in water and thus water-d_2/methanol-d_4 mixture and acetonitrile-d_3 were
416 used as solvents. The basic sites were then determined by titration of the appropriate solutions of the
417 samples with equivalent amounts of deutero-trifluoroacetic acid (TFA-d) solution.

SM07

419 5.8 mg of SM07 was dissolved in 600 µL of methanol-d_4:water-d_2 (2:1 v/v ratio). A 9% v/v TFA-d solution
420 in water-d2 was prepared, such that each 20 µL volume contained approximately 1 equivalent of TFA-d
421 with respect to the base. SM07 solution was then titrated with the TFA-d solution at 0.5, 1.0, 1.5, and 5.0
422 equivalents with a ^{1}H-^{15}N HMBC spectra (optimized for 5 Hz) acquired after each TFA addition. A reference
423 ^{1}H-^{15}N HMBC experiment was first acquired on the SM07 solution prior to commencement of the titration.

SM14

425 5.5 mg of SM14 was dissolved in 600 µL of acetonitrile-d_3. A 10% v/v TFA-d solution in acetonitrile-d_3 was
426 prepared, 20 µL of which corresponds to 1 equivalent of TFA-d with respect to the base. Further 1:10 dilution
427 of the TFA-d solution in acetonitrile-d_3, allowed measurement of 0.1 equivalent of TFA-d per 20 µL of solution.
428 SM14 solution was then titrated with the TFA-d solutions at 0.0, 0.5, 1.0, 1.1, 1.2, 1.3, 1.5, 1.8, 2.0, 2.1, 2.6, 5.1,
429 and 10.1 equivalents. The chemical shift changes were monitored by the acquisition of ^{1}H-^{15}N HMBC spectra
430 (optimized for 5 Hz) after each TFA addition.

Results

Spectrophotometric pK_a measurements

433 Spectrophotometrically-determined pK_a values for all molecules from the SAMPL6 pK_a challenge are shown
434 in Figure 6 and Table 1. The protocol used—cosolvent or aqueous UV-metric titration—is indicated in
435 Table 1 together with SEM of each reported measurement. Out of 24 molecules successfully assayed, five
436 molecules have two resolvable pK_a values, while one has three resolvable pK_a values within the measurable
437 pK_a range of 2–12. The SEM of reported pK_a measurements is low, with the largest uncertainty reported
438 being 0.04 pK units (pK_{a1} of SM06 and pK_{a3} of SM18). Individual replicate measurements can be found in
439 Supplementary Table 3. Reports generated for each pK_a measurement by the Sirius T3 Refine software can
440 also be found in the Supplementary Information. Experimental pK_a values for nearly all compounds with
441 multiple resolvable pK_as are well-separated (more than 3 pK_a units), except for SM14 and SM18.

Impact of cosolvent to UV-metric pK_a measurements

443 For molecules with insufficient aqueous solubilities throughout the titration range (pH 2–12), we resorted
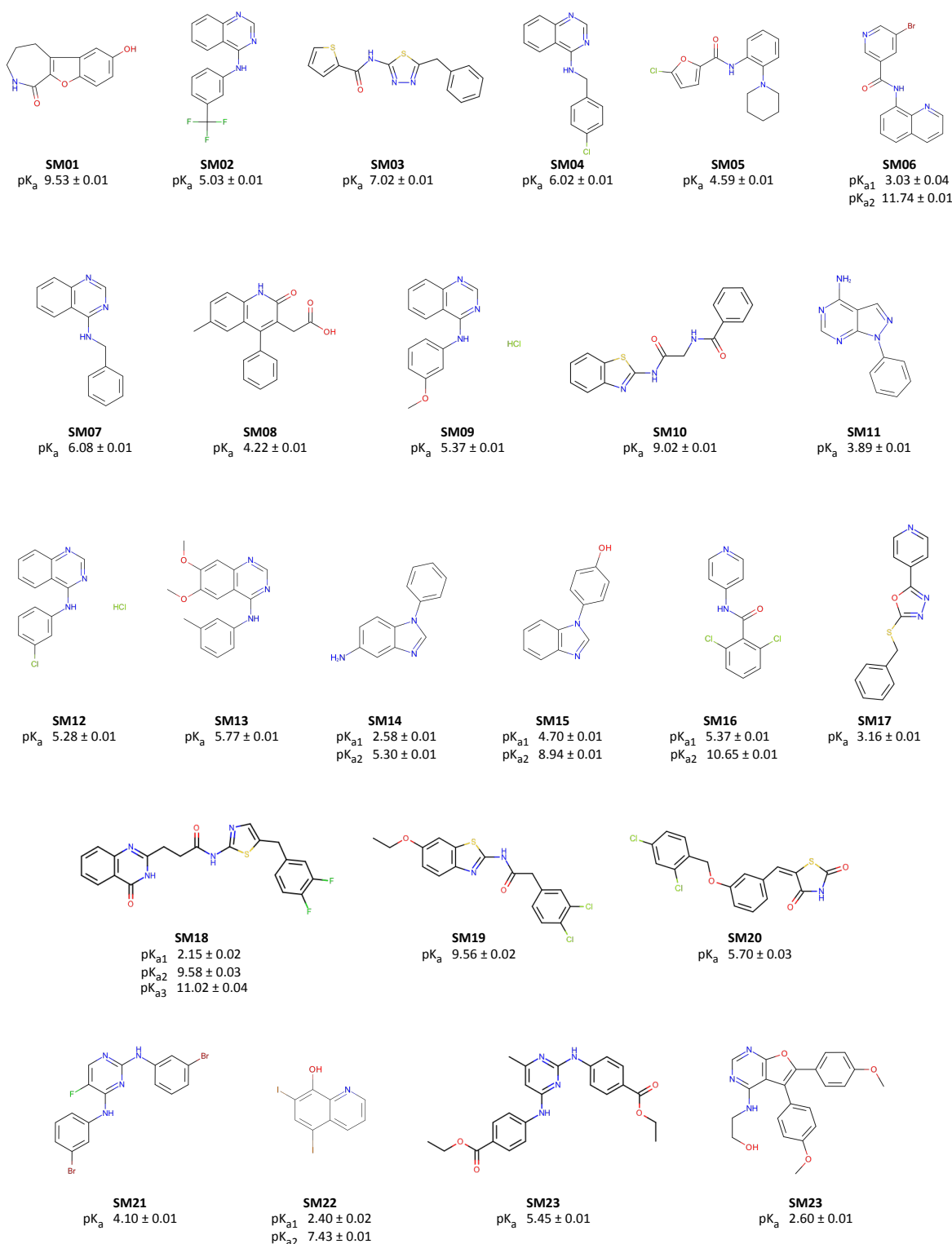444 to cosolvent UV-metric pK_a measurements, with methanol used as cosolvent. To confirm that cosolvent

Figure 6. Molecules used in the SAMPL6 pK_a challenge. Experimental UV-metric pK_a measurements were performed for these 24 molecules and discernable macroscopic pK_as are reported. Uncertainties are expressed as the standard error of the mean (SEM) of three independent measurements. We depicted neutral states of the molecules as sites of protonation were not determined by UV-metric methods. 2D structures were created with OpenEye OEDepict Toolkit [57]

Table 1. Experimental pK$_a$s of SAMPL6 compounds. Spectrophotometric pK$_a$ measurements were performed with two assay types based on aqueous solubility of analytes. "UV-metric pK$_a$" assay indicates spectrophotometric pK$_a$ measurements done with Sirius T3 in ISA water. "UV-metric pK$_a$ with cosolvent" assay refers to pK$_a$ determination by Yasuda-Shedlovsky extrapolation from p$_s$K$_a$ measurements in various ratios of ISA methanol:water mixtures. Triplicate measurements were performed at $25 \pm 0.5°$ C and in the presence of approximately 150 mM KCl to adjust ionic strength.

Molecule ID	pK$_{a1}$	pK$_{a2}$	pK$_{a3}$	Assay Type
SM01	9.53 ± 0.01			UV-metric pK$_a$
SM02	5.03 ± 0.01			UV-metric pK$_a$ with cosolvent
SM03	7.02 ± 0.01			UV-metric pK$_a$ with cosolvent
SM04	6.02 ± 0.01			UV-metric pK$_a$
SM05	4.59 ± 0.01			UV-metric pK$_a$ with cosolvent
SM06	3.03 ± 0.04	11.74 ± 0.01		UV-metric pK$_a$
SM07	6.08 ± 0.01			UV-metric pK$_a$
SM08	4.22 ± 0.01			UV-metric pK$_a$
SM09	5.37 ± 0.01			UV-metric pK$_a$ with cosolvent
SM10	9.02 ± 0.01			UV-metric pK$_a$ with cosolvent
SM11	3.89 ± 0.01			UV-metric pK$_a$
SM12	5.28 ± 0.01			UV-metric pK$_a$
SM13	5.77 ± 0.01			UV-metric pK$_a$
SM14	2.58 ± 0.01	5.30 ± 0.01		UV-metric pK$_a$
SM15	4.70 ± 0.01	8.94 ± 0.01		UV-metric pK$_a$
SM16	5.37 ± 0.01	10.65 ± 0.01		UV-metric pK$_a$
SM17	3.16 ± 0.01			UV-metric pK$_a$
SM18	2.15 ± 0.02	9.58 ± 0.03	11.02 ± 0.04	UV-metric pK$_a$ with cosolvent
SM19	9.56 ± 0.02			UV-metric pK$_a$ with cosolvent
SM20	5.70 ± 0.03			UV-metric pK$_a$ with cosolvent
SM21	4.10 ± 0.01			UV-metric pK$_a$ with cosolvent
SM22	2.40 ± 0.02	7.43 ± 0.01		UV-metric pK$_a$ with cosolvent
SM23	5.45 ± 0.01			UV-metric pK$_a$ with cosolvent
SM24	2.60 ± 0.01			UV-metric pK$_a$ with cosolvent

[1] pK$_a$ values are reported as mean $\pm$ SEM of three replicates.

UV-metric pK$_a$ measurements led to indistinguishable results compared to aqueous UV-metric measurements, we collected pK$_a$ values of 12 highly soluble SAMPL6 compounds—as well as pyridoxine—using both cosolvent and aqueous methods. Correlation analysis of pK$_a$ values determined with both methods demonstrated that using methanol as cosolvent and determining aqueous pK$_a$s via Yasuda-Shedlovsky extrapolation did not result in significant bias (Figure 7), since 95% CI for mean deviation (MD) between two measurements includes zero. Means and standard errors of UV-metric pK$_a$ measurements with and without cosolvent are provided in Supplementary Table 5. pK$_a$ measurement results of individual replicate measurements with and without cosolvent can be found in Supplementary Table 4.

Purity of SAMPL6 compounds

LC-MS based purity measurements showed that powder stocks of 23 of the SAMPL6 pK$_a$ challenge compounds were >90% pure, while purity of SM22 was 87%—the lowest in the set (Supplementary Table 6). Additionally, molecular weights detected by LC-MS method were consistent with those reported in eMolecules, as well as supplier-reported molecular weights, when provided. It is recommended by Sirius/Pion technical specialists to use compounds with ~90% purity to minimize the impact on high-accuracy pK$_a$ measurements. Impurities with no UV-chromophore, or elute too late in LC may not be detected with this method, although
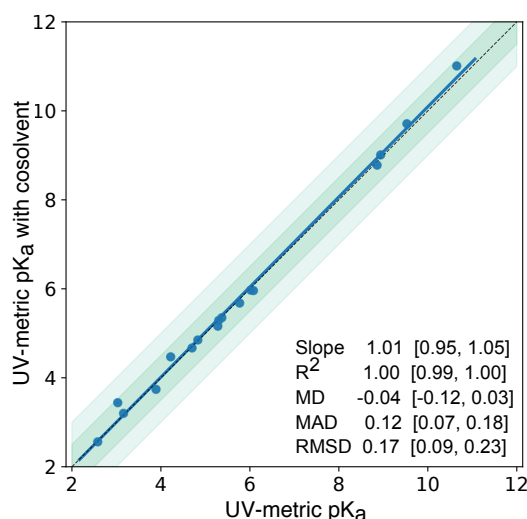
Figure 7. pK_a measurements with UV-metric method with cosolvent and UV-metric method in water show good correlation. 17 pK_a values (blue marks) of 13 chemicals were measured with both UV-metric pK_a method in water and UV-metric pK_a method with methanol as cosolvent (Yasuda-Shedlovsky extrapolation to 0% methanol). Dashed black line has slope of 1, representing perfect correlation. Dark and light green shaded areas indicate $\pm$0.5 and $\pm$1.0 pK_a unit difference regions, respectively. Error bars are plotted as the SEM of replicate measurements, although they are not visible since the largest SEM is 0.04. MD: Mean difference, MAD: Mean absolute deviation, RMSD: Root-mean-square deviation. Confidence intervals (reported in brackets) report the 95%ile CI calculated over 10 000 bootstrap samples. Experimental data used in this plot is reported in Supplementary Table 4.

460 chances are small. The peak purity check of primary peak can detect the presence of a large impurity
461 underneath the main peak, but if the UV spectrum of the impurity is exactly same with analyte in the main
462 peak, it may not be resolved. HPLC UV detector's wavelength inaccuracy is <1%. Mass inaccuracy of MS
463 instrument is ~0.13 um within the calibrated mass range in the scan mode.

Characterization of SM07 microstates with NMR

465 [15]N Chemical shifts (ppm, referenced to ammonia at 0 ppm) for N-8, N-10 and N-12—measured from
466 the ^{1}H-^{15}N HMBC experiments—were plotted against the titrated TFA-d equivalents (0.0, 0.5, 1.0, 1.5, and
467 5.0 equivalents) (Figure 8 A). A large upfield shift of ~82 ppm is observed for N-12. The initial linear
468 relationship between chemical shift and TFA equivalents, shown in Figure SI 25 for N-12, is expected for
469 strong monoprotic bases—as is the case for SM07. The large upfield chemical shift change (82 ppm) is
470 consistent with a charge delocalization as shown in the resonance structures inset of Figure SI 25. Further
471 evidence for this delocalization is observed for N-8, which shows a downfield chemical shift change of ~28
472 ppm compared to just ~1.5 ppm for N-10. Titration of SM07 with more than 1 equivalents of TFA-d did not
473 result in further significant chemical shift changes—establishing that SM07 is a monoprotic base(Figure 8A).

Characterization of SM14 microstates with NMR

475 Determining the protonation sites for SM14, which has pK_a values of 2.58 and 5.30 (Table 1), was more
476 challenging due to multiple possible resonance structures in the mono- and di-protonated states. We noticed
477 that water/methanol co-solvent exhibited strong solvent effects, which complicated the data interpretation
478 for SM14. For instance, titration of SM14 in methanol/water (see SI) showed incomplete protonation of
479 N-9 even after 5 equivalents of TFA-d were added. This observation is consistent with UV-metric p$_s K_a$
480 measurements done in methanol cosolvent, where both p$_s K_a$ values were decreasing as the percentage of
481 methanol was increased, making observation of these protonation states more difficult. Thus the utilization
482 of an aprotic solvent was necessary for unambiguous interpretation of the data.

483 Acetonitrile-d_3 was selected as our solvent of choice. Titration of SM14 (5.5 mg) with up to 10 equivalents
484 of TFA-d in acetonitrile-d_3 (0.0, 0.5, 1.0, 1.1, 1.2, 1.3, 1.5, 1.8, 2.0, 2.1, 2.6, 5.1, and 10.1 equivalents), provided
485 a much clearer picture of its protonation states (Figure 8 B). N-9, with the large upfield chemical shift change
486 ~72 ppm at 1 equivalent of TFA-d, clearly is the site of first protonation. At this point, the downfield chemical
487 shift changes observed for N-7 ($\Delta\delta \approx 6.5$) and N-16 ($\Delta\delta \approx 5$) can be attributed to electronic effects rather than
488 a direct protonation. The large upfield shift for N-9 indicates this to be the site of first protonation; complete
489 protonation was attained at roughly 2.5 equivalents of TFA-d, suggesting that SM14 is a weak base under
490 these experimental conditions. Following the protonation of N-9, a second protonation event occurs at N-16
491 nitrogen as evident by the upfield chemical shift change observed for N-16. However, a continuous change
492 in the chemical shift of N-16 even after addition of 10 equivalents of TFA-d indicates that this protonation
493 event is incomplete but provides evidence for N-16 being the second protonation site. This observation is
494 consistent with N-16 being even a weaker base than N-9, which is expected of the aniline-type amines. Other
495 notable observations are the slight downfield chemical shift changes for N-7 and N-9, during the second
496 protonation event. This is attributed to electronic effects from the protonation of N-16.

Discussion

Sample preparation and effect of cosolvents in UV-metric measurements

499 Samples for UV-metric pK_a measurements were prepared by dilution of up to 5 µL DMSO stock solution
500 of analyte in 1.5 mL ISA water, which results in the presence of ~0.3% DMSO during titration, which is
501 presumed to have a negligible effect on pK_a measurements. For UV-metric or pH-metric measurements, it is
502 possible to prepare samples without DMSO, but it is difficult to prepare samples by weighing extremely low
503 amounts of solid stocks (in the order of 0.01–0.10 mg) to target 50 µM analyte concentrations, even with
504 an analytical balance. For experimental throughput, we therefore preferred using DMSO stock solutions.
505 Another advantage of starting from DMSO stock solutions is that it helps to overcome kinetic solubility
506 problems of analytes.

507 In UV-metric measurements, both water and methanol (when used as cosolvent) stock solutions were
508 ionic strength adjusted with 150 mM KCl, but acid and base solutions were not. This means that throughout
509 pH titration ionic strength slighly fluctuates, but on average ionic strength of samples were staying around
510 150–180 mM. By using ISA solutions the effect of salt concentration change on pK_a measurements was
511 minimized.

512 If an analyte is soluble enough, UV-metric pK_a measurements in water should be preferred over cosolvent
513 methods, since pK_a measurement in water is more direct. For pK_a determination via cosolvent extrapolation
514 using methanol, the apparent pK_as (p$_s$$K_a$) in at least three different methanol:water ratios must be measured,
515 and the pK_a in 0% cosolvent computed by Yasuda-Shedlovsky extrapolation. The number and spread of
516 p$_s$$K_a$ measurements and error in linear fit extrapolation influences the accuracy of pK_as determined by this
517 approach. To test that UV-metric methods with or without cosolvent have indistinguishable performance,
518 we collected pK_a values for 17 SAMPL6 compounds and pyridoxine with both methods. Figure 7 shows there
519 is good correlation between both methods and the mean absolute deviation between two methods is 0.12
520 (95% CI [0.07, 0.18]). The mean deviation between the two sets is -0.04 (95% CI [-0.12, 0.03]), showing there is
521 no significant bias in cosolvent measurements as the 95% CI includes zero. The largest absolute deviation
522 observed was 0.41 for SM06.

Impact of impurities to UV-metric pK_a measurements

524 Precisely how much the presence of small amounts of impurities impact UV-metric pK_a measurements is
525 unpredictable. For an impurity to alter UV-metric pK_a measurements, it must possess a UV-chromophore and
526 a titratable group in the vicinity of the chromophore—otherwise, it would not interfere with absorbance signal
527 of the analyte. If a titratable impurity *does* possess a UV-chromophore, UV multiwavelength absorbance
528 from the analyte and impurity will be convoluted. How much the presence of impurity will impact the
529 multiwavelength absorbance spectra and pK_a determination depends on the strength of the impurity's molar
530 absorption coefficient and concentration, relative to the analyte's. In the worst case scenario, an impurity
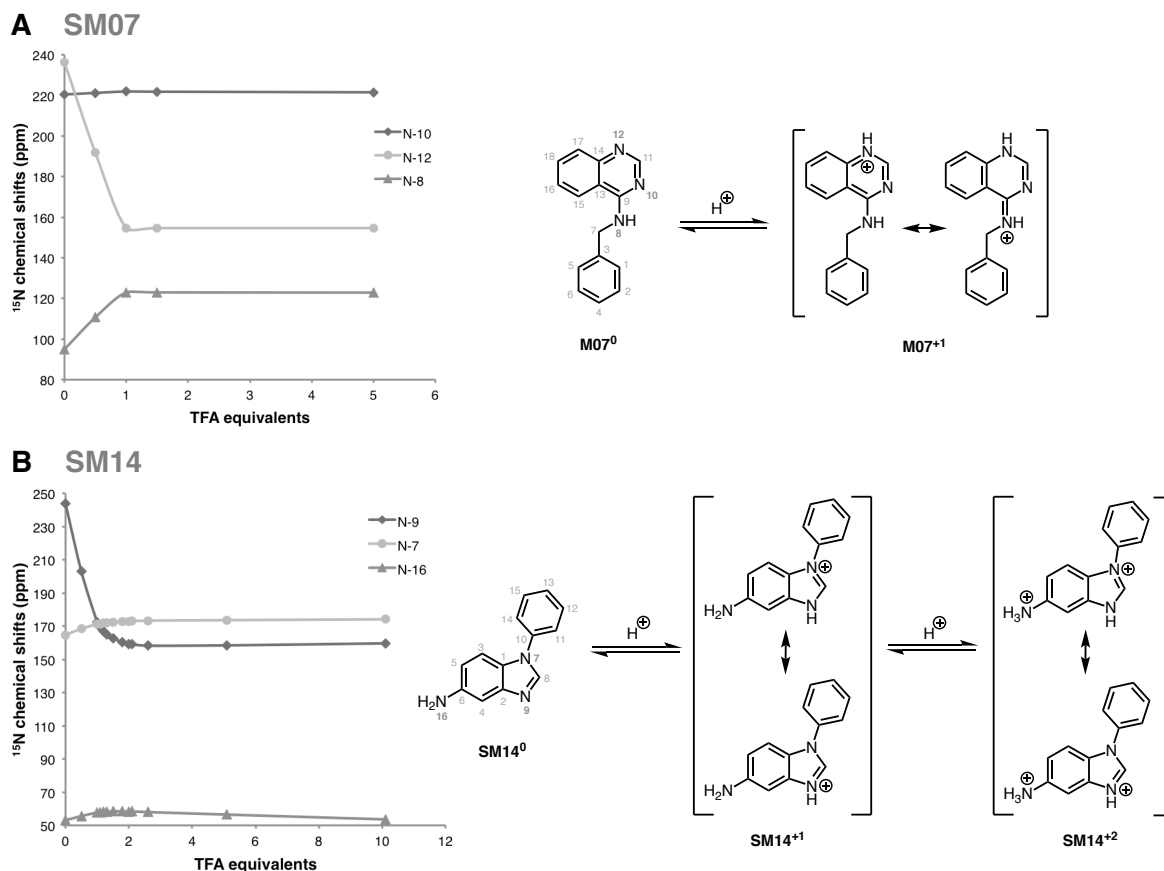
A SM07

B SM14

Figure 8. Dominant protonation microstates of SM07 and SM14 characterized by NMR. (A) Sequence of protonation sites of SM07 were determined by ^{1}H-^{15}N HMBC experiments in 1:2 water:methanol mixture. *Left:* The plot of ^{15}N chemical shifts of N-10, N-12, and N-8 of SM07 *vs* titrated TFA-*d* equivalents, showing the mono-protonation of N-12 as evidenced by its large upfield chemical shifts change. Acidity of the medium increases as more equivalents of TFA-*d* were added. Electronic effects due to protonation of N-12 cause downfield chemical shift change of N-10 and N-8 between 0–1 equivalents of TFA-*d*. *Right:* NMR-based model of the order of dominant protonation states for M07. Only one protonation event was observed, at N-12. Microstates shown in the figure are the most likely contributors to the UV-metric pK_a of 6.08 ± 0.01. **(B)** Sequence of protonation sites of SM14 were determined by ^{1}H-^{15}N HMBC experiments in acetonitrile. *Left:* The plot of ^{15}N chemical shifts of N-9, N-7, and N-16 of SM14 *vs* titrations of TFA-*d* equivalents, showing two sequential protonation events. The first protonation at N-9 with a large upfield chemical shift change of 71.6 ppm was seen between 0–1 equivalents of TFA-*d*. Downfield chemical shift change of N-7 and N-19 in this region were due the electronic effect from the protonation of N-9. N-16 also exhibited a small upfield chemical shift change of 4.4 ppm between 2.5–10 equivalents of TFA-*d*, which indicated N-16 as the second site of protonation. *Right:* NMR based model of the order of dominant protonation states for M14, showing two sequential protonation events. Also, two pK_a values were detected with UV-metric pK_a measurements for SM14. Assuming sequence of protonation events will be conserved between water and acetonitrile solvents, SM14[0] and SM14[+1] microstates shown in the figure are the major contributors to the UV-metric pK_a value 5.30 ± 0.01. SM14[+1] and SM14[+2] microstates shown in the figure are the major pair of microstates contributing to the UV-metric pK_a value 2.58 ± 0.01. There could be minor microstates with very low populations that could not be distinguished in these NMR experiments.

531 with high concentration or strong UV absorbance can shift the measured pK_a value or create the appearance
532 of an extra pK_a. As a result, it is important to use analytes with high purities to obtain high accuracy pK_a
533 measurements. Therefore, we confirmed the purities of SAMPL6 compounds with LC-MS.

Interpretation of UV-metric pK_a measurements

535 Multiwavelength absorbance analysis on the Sirius T3 allows for good resolution of pK_as based on UV-
536 absorbance change with respect to pH, but it is important to note that this method potentially produces
537 *macroscopic* pK_as for polyprotic compounds. If multiple microscopic pK_as have close pK_a values and overlap-
538 ping changes in UV absorbance spectra associated with protonation/deprotonation, the spectral analysis
539 could produce a single macroscopic pK_a that represents an aggregation of multiple microscopic pK_as. An
540 extreme example of such case is demonstrated in the simulated macrostate populations of cetirizine that
541 would be observed with UV-metric titration (Figure 2).

542   If protonation state populations observed via UV-metric titrations (such as in Figure 3B) are composed
543 of a single microstate, experimentally measured pK_as are indeed microscopic pK_as. Unfortunately, judging
544 the composition of experimental populations is not possible by just using UV-metric or pH-metric titration.
545 Molecules in the SAMPL6 pK_a challenge dataset with only one pK_a value measured in the 2–12 range could
546 therefore be monoprotic (possessing a single titratable group that changes protonation state by gain or
547 loss of a single proton over this pH range) or polyprotic (gaining or losing multiple protons from one or
548 more sites with overlapping microscopic pK_a values). Similarly, titration curves of molecules with multiple
549 experimental pK_as may show well-separated microscopic pK_as or macroscopic experimental pK_as that
550 are really composites of microscopic pK_as with similar values. Therefore, without additional experimental
551 evidence, UV-metric pK_as should not be assigned to individual titratable groups.

552   Determination of the exact microstates populated at different pH values via NMR can provide a com-
553 plementary means of differentiating between microscopic and macroscopic pK_as in cases where there is
554 ambiguity. As determination of protonation microstates via NMR is very laborious, we were only able to
555 characterize microstates of two molecules: SM07 and SM11.

556   In UV-metric pK_a measurements with cosolvent, the slope of the Yasuda-Shedlovsky extrapolation can
557 be interpreted to understand if the pK_a has dominantly acidic or basic character. As the methanol ratio
558 is increased, p$_s K_a$ values of acids increase, while p$_s K_a$ values for bases decrease. However, it is important
559 to remember that if the measured pK_a is macroscopic, acid/base assignment from cosolvent p$_s K_a$ trends
560 is also a macroscopic property, and should not be used as a guide for assigning pK_a values to functional
561 groups [58].

NMR microstate characterization

563 The goal of NMR characterization was to collect information on microscopic states related to experimental
564 pK_a measurements, i.e., determine exact sites of protonation. pK_a measurements performed with spec-
565 trophotometric method provide macroscopic pK_a values, but do not provide information on the site(s) of
566 protonation. On the other hand, most computational prediction methods primarily predict microscopic
567 pK_a values. Protonation sites can be determined by NMR methods, although these measurements are
568 very laborious in terms of data collection and interpretation compared to pK_a measurements with the
569 automated Sirius T3. Moreover, not all SAMPL6 molecules were suitable for NMR measurements due to the
570 high sample concentration requirements (for methods other than proton NMR, such as ^{13}C and ^{15}N spectra)
571 and limiting analyte solubility. Heavy atom spectra that rely on natural isotope abundance require high
572 sample concentrations (preferably in the order of 100 mM). It is possible that drug or drug-fragment-like
573 compounds, such as the compounds used in this study, have insufficient aqueous solubility, limiting the
574 choice of solvent and pH. It may be necessary to use organic cosolvents to prepare these high concentration
575 solutions or only prepare samples at pH values that correspond to high solubility states (e.g., when the
576 charged state of the compound is populated).

577   We performed NMR based microstate characterization only for SM07 and SM14. We were able to identify
578 the order of dominant protonation microstates, as shown in Figure 8. These pairs of microstates and
579 the order of microscopic transitions can be associated with experimental pK_as determined by UV-metric

titrations, under the assumption that different organic solvents used in NMR measurements will have negligible effect on the sequence of microstates observed as the medium was titrated with acid, although shift in pK_a values is expected. NMR measurements for SM07 and SM14 were done in water:methanol (1:2 (v/v)) and acetonitrile solutions, respectively. On the other hand, pK_a values of these two compounds were determined by UV-metric titrations in ISA water. Additional UV-metric pK_a measurements of these compounds with methanol as cosolvent showed that their p$_s K_a$ values decreased as the cosolvent ratio increased (i.e., dielectric constant decreased) as expected from base titration sites. Identification of SM07 and SM14 titratable sites type as base is consistent between NMR based models and UV-metric cosolvent titrations. The order of microstates observed in the titration of NMR samples are very likely to corresponds to the dominant microstates associated with UV-metric pK_a measurements. N-12 of SM07 was observed as the only protonation site of SM07 during TFA-*d* titration up to 5 equivalents which supports that SM07 is a mono-protic acid and UV-metric pK_a value 6.08 ± 0.01 corresponds to microscopic protonation of N-12. For SM14, two protonation sites were observed (N-16 and N-9, in the order of increasing p$_s K_a$). Microstate pairs shown in Figure 8B were determined as dominant contributors to UV-metric pK_as 2.58 ± 0.01 and 5.30 ± 0.01, although minor microspecies with very low populations (undetected in NMR experiments) could be contributing to macroscopic pK_a values observed by UV-metric method.

In addition to SM07, there were five other 4-aminoquinazoline derivatives in the SAMPL6 set: SM02, SM04. SM09, SM12, and SM13. For these series, all the potential titratable sites are located in 4-aminoquinazoline scaffold and there are no other additional titratable sites present in these compounds compared to SM07. Therefore, based on structural similarity, it is reasonable to predict that N-12 is the microscopic protonation site for all of these compounds. We can infer that UV-metric pK_a values measured for the 4-aminoquinazoline series are also microscopic pK_as and they are related to the protonation of the same quinazoline nitrogen with the same neutral background protonation states as shown for SM07 in Figure 8A.

Recommendations for future pK_a prediction challenges

Most high-throughput pK_a measurement methods measure macroscopic pK_as. One way to circumvent this problem is to confine our interest in future pK_a challenges to experimental datasets containing only monoprotic compounds if UV-metric or pH-metric pK_a measurements are the method of choice, allowing unambiguous assignment of pK_a values to underlying protonation states. However, it is important to consider that multiprotic compounds are common in pharmaceutically interesting molecules, necessitating the ability to model them reliably. It might also be interesting to select a series of a polyprotic compounds and their monoprotic fragments, to see if they can be used to disambiguate the pK_a values.

Although relatively efficient, UV-metric pK_a measurements with the Sirius T3 do not provide structural information about microstates. Even the acid-base assignment based on direction of p$_s K_a$ shift with cosolvent is not a reliable indicator for assigning experimental pK_a values to individual functional groups in multiprotic compounds. On the other hand, most computational pK_a prediction methods output microscopic pK_as. It is therefore difficult to use experimental macroscopic pK_a values to assess and train microscopic pK_a prediction methods directly without further means of annotating macroscopic-microscopic correspondence. It is not straight-forward to infer the underlying microscopic pK_a values from macroscopic measurements of a polyprotic compound without complementary experiments that can provide structural information. Therefore, for future data collection efforts for evaluation of pK_a predictions, if measurement of pK_as via NMR is not possible, we advise supplementing UV-metric measurements with NMR characterization of microstates to show if observed pK_as are microscopic (related to a single group) or macroscopic (related to dissociation of multiple groups), as performed for SM07 and SM14 in this study.

Another source of complexity in interpreting macroscopic pK_a values is how the composition of macroscopic pK_as can change between different experimental methods as illustrated in Figure 2. Different subsets of microstates can become indistinguishable based on the type of signal the experimental method is constructed on. In potentiometric titrations, microstates with the same total charge are indistinguishable and are observed as one macroscopic population. In spectrophotometric pKa measurements, microstates whose populations, and therefore UV-absorbance spectra, change around the same pH value become indistinguishable.

The "macroscopic" label is commonly ascribed to transitions between different ionization states of a molecule (all microstates that have the same total charge form one macrostate), but this definition only applies to potentiometric methods. In UV-absorbance based methods, the principle that determines which microstates will be distinguishable is not charge or number of bound protons, but molecular absorbance changes, and how closely underlying microscopic pK_a values overlap. To compare experimental macroscopic pK_a and microscopic computational predictions on common ground, the best solution is to compute "predicted" macroscopic pK_a values from microscopic pK_as based on the detection limitations of the experiment. A disadvantage of this approach is that experimental data cannot provide direct guidance on microscopic pK_a resolution for improving pK_a prediction methods.

Since analyte purity is critical for accuracy, necessary quality control experiments must be performed to ensure at least 90% purity for UV-metric pK_a measurements. Higher purities may be necessary for other methods. For potentiometric methods, knowing the stoichiometry of any counterions present in the original powder stocks is also necessary. Identity of counterions also needs to be known to incorporate titratable counterions, e.g. ammonia in the titration model.

For the set of SAMPL6 pK_a challenge compounds, we could not use potentiometric pK_a measurements due to the low aqueous solubility of many of these compounds. The lowest solubility observed *somewhere* in the experimental pH range of titration is the limiting factor, since for accurate measurements the analyte must stay in the solution phase throughout the entire titration. Since the titration pH range is determined with the goal of capturing all ionization states, the analyte is inevitably exposed to pH values that correspond to low solubility. Neutral and zwitterionic species can be orders of magnitude less soluble than ionic species.

For future pK_a challenges with multiprotic compounds, if sufficient time and effort can be spared, it would be ideal to construct an experimental pK_a dataset using experimental methods that can measure microscopic pK_as directly, such as NMR. In the present study, we were only able to perform follow up NMR microstate characterization of two compounds because we relied on intrinsically low-sensitivity and time-consuming ^{1}H-^{15}N HMBC experiment at natural abundance of ^{15}N nuclei. ^{1}H-^{15}N HMBC experiments of SM07 and SM14 required high analyte concentrations and thus the use of organic solvents for solubility. Alternatively, it might be possible to determine microstates with ^{1}H-NMR by analyzing chemical shift changes of reporter protons [21] in aqueous solutions with lower analyte concentrations and with much higher throughput than ^{15}N-based experiments. However, it should be noted that ^{1}H NMR titration data may not always be sufficient for unambiguous microstate characterization. In this case, other reporter nuclei such as ^{13}C, ^{19}F and ^{31}P can be used where appropriate to supplement ^{1}H data To prepare sample solutions for NMR at specific pH conditions, the Sirius T3 can be used to automate the pH adjustment of samples. Another advantage of using the Sirius T3 for NMR sample preparation includes preparing ionic strength adjusted NMR samples and minimizing consumption of the analyte since small volumes (as low as 1.5 mL) of pH adjusted solutions can be prepared.

In the future pK_a challenges, it would be especially interesting to expand this exercise to larger and more flexible drug-like molecules. pK_a values are environment dependent and it would be useful to be able to predict pK_a shifts based on on ionic strength, temperature, lipophilic content, with cosolvents or in organic solvents. Measuring the pK_a of molecules in organic solvents would be useful for guiding process chemistry. To test such predictions, special pK_a experiments would need to be designed to measure pK_as under different conditions.

The next iteration of the SAMPL log D prediction challenge will include a subset of compounds from pK_a challenge. We therefore envision that the collected dataset of pK_a measurements will also be of use for this challenge. Experimental pK_a values will be provided as an input to separate the pK_a prediction issue from other problems related to log D predictions. We expect that the experimental pK_as can be used as an indication if protonation states need to be taken into account for a log D prediction at a certain pH and for the validation of protonation state population predictions in the aqueous phase. Even for compounds for which microstates were not experimentally determined, macroscopic pK_a value can serve as an indicator of how likely it is that protonation states will have a significant effect on the log D of a molecule. Additionally, the information from NMR experiments in this study provided the site of protonation for six 4-aminoquinazoline compounds, which could be incorporated as microstate information for log D predictions. For predicting

681 log D we suggest as a rule of thumb to include protonation state effects for pK_a values at least within 2
682 units of the pH of the log D experiment. pK_a values of six 4-aminoquinazoline compounds in this study were
683 determined to be within 2 pKa units from 7.

Conclusion

685 This study reports the collection of experimental data for the SAMPL6 pK_a prediction challenge. Collection of
686 experimental pK_a data was performed with the goal of evaluating computational pK_a predictions, therefore
687 necessary quality control and uncertainty propagation measures were incorporated. The challenge was
688 constructed for a set of fragment-like and drug-like small molecules, selected from kinase-targeted chemical
689 libraries, resulting in a set of compounds containing heterocycles frequently found in FDA-approved kinase
690 inhibitors. We collected pK_a values for 24 compounds with the Sirius T3 UV-metric titration method, which
691 were then used as the experimental reference dataset for the SAMPL6 pK_a challenge. For compounds with
692 poor aqueous solubilities we were able to use the Yasuda-Shedlovsky extrapolation method to measure pK_a
693 values in the presence of methanol, and extrapolate to a purely aqueous phase.

694 In our work, we highlighted the distinction between microscopic and macroscopic pK_as which is based
695 on the experimental method used, especially how underlying microstate composition can be different for
696 macroscopic pK_as measured with UV-metric vs pH-metric titration methods. We discuss how macroscopic pK_a
697 values, determined by UV, introduce an identifiability problem when comparing to microscopic computational
698 predictions. For two compounds (SM07 and SM14) we were able to alleviate this problem by determining
699 the sequence of microscopic protonation states using ^{1}H-^{15}N HMBC experiments. Microstates of five other
700 compounds with 4-aminoquinazoline scaffold were inferred based on the NMR characterization of SM07
701 microstates which showed that it is monoprotic.

702 The collected experimental data constitute a potentially useful dataset for future evaluation of small
703 molecule pK_a predictions, even outside of SAMPL challenges. We expect that this data will also be useful for
704 participants in the next SAMPL challenge on small molecule lipophilicity predictions.

Code and data availability

706
- SAMPL6 pK_a challenge instructions, submissions, experimental data and analysis is available at
  https://github.com/MobleyLab/SAMPL6
- Python scripts used for compound selection are available at **compound_selection** directory of
  https://github.com/choderalab/sampl6-physicochemical-properties

Overview of supplementary information

708 Organized in SI document:
709 - TABLE SI 1: Procurement details of SAMPL6 compounds
710 - TABLE SI 2: Selection details of SAMPL6 compounds
711 - TABLE SI 3: pK_a results of replicate experiments CSV
712 - TABLE SI 4: pK_a results of water and cosolvent replicate experiments CSV
713 - TABLE SI 5: pK_a mean and SEM results of water and cosolvent replicate experiments
714 - TABLE SI 6: Summary of LC-MS purity results
715 - FIGURE SI 1 - 24: LC-MS Figures
716 - FIGURE SI 25: NMR characterization of SM07 microstates
717 - FIGURE SI 26: NMR characterization of SM014 microstates

718 Extra files:
719 - Sirius T3 reports: `supplementary_files.zip`

Author Contributions

721 Conceptualization, MI, JDC, TR, ASR, DLM ; Methodology, MI, DL, IEN ; Software, MI, ASR ; Formal Analysis, MI ;
722 Investigation, MI, DL, IEN, HW, XW, MR; Resources, TR, DL; Data Curation, MI ; Writing-Original Draft, MI, JDC,

IEN; Writing - Review and Editing, MI, DL, ASR, IEN, HW, XW, MR, GEM, DLM, TR, JDC; Visualization, MI, IEN ; Supervision, JDC, TR, DLM, GEM, AAM ; Project Administration, MI ; Funding Acquisition, JDC, DLM, TR, MI.

Acknowledgments

Disclosures

JDC is a member of the Scientific Advisory Board for Schrödinger, LLC. DLM is a member of the Scientific Advisory Board of OpenEye Scientific Software.

References

[1] **Mobley DL**, Chodera JD, Isaacs L, Gibb BC. Advancing predictive modeling through focused development of model systems to drive new modeling innovations. UC Irvine: Department of Pharmaceutical Sciences, UCI. 2016; https://escholarship.org/uc/item/7cf8c6cr.

[2] **Drug Design Data Resource**, SAMPL;. https://drugdesigndata.org/about/sampl.

[3] **Nicholls A**, Mobley DL, Guthrie JP, Chodera JD, Bayly CI, Cooper MD, Pande VS. Predicting Small-Molecule Solvation Free Energies: An Informal Blind Test for Computational Chemistry. J Med Chem. 2008 Feb; 51(4):769–779. doi: 10.1021/jm070549+.

[4] **Guthrie JP**. A Blind Challenge for Computational Solvation Free Energies: Introduction and Overview. J Phys Chem B. 2009 Jan; 113(14):4501–4507.

[5] **Skillman AG**, Geballe MT, Nicholls A. SAMPL2 Challenge: Prediction of Solvation Energies and Tautomer Ratios. J Comput Aided Mol Des. 2010 Apr; 24(4):257–258. doi: 10.1007/s10822-010-9358-0.

[6] **Geballe MT**, Skillman AG, Nicholls A, Guthrie JP, Taylor PJ. The SAMPL2 Blind Prediction Challenge: Introduction and Overview. J Comput Aided Mol Des. 2010 May; 24(4):259–279. doi: 10.1007/s10822-010-9350-8.

[7] **Skillman AG**. SAMPL3: Blinded Prediction of Host–guest Binding Affinities, Hydration Free Energies, and Trypsin Inhibitors. J Comput Aided Mol Des. 2012 May; 26(5):473–474. doi: 10.1007/s10822-012-9580-z.

[8] **Geballe MT**, Guthrie JP. The SAMPL3 Blind Prediction Challenge: Transfer Energy Overview. J Comput Aided Mol Des. 2012 Apr; 26(5):489–496. doi: 10.1007/s10822-012-9568-8.

[9] **Muddana HS**, Varnado CD, Bielawski CW, Urbach AR, Isaacs L, Geballe MT, Gilson MK. Blind Prediction of Host–guest Binding Affinities: A New SAMPL3 Challenge. J Comput Aided Mol Des. 2012 Feb; 26(5):475–487. doi: 10.1007/s10822-012-9554-1.

[10] **Guthrie JP**. SAMPL4, a Blind Challenge for Computational Solvation Free Energies: The Compounds Considered. J Comput Aided Mol Des. 2014 Apr; 28(3):151–168. doi: 10.1007/s10822-014-9738-y.

[11] **Mobley DL**, Wymer KL, Lim NM, Guthrie JP. Blind Prediction of Solvation Free Energies from the SAMPL4 Challenge. J Comput Aided Mol Des. 2014 Mar; 28(3):135–150. doi: 10.1007/s10822-014-9718-2.

[12] **Muddana HS**, Fenley AT, Mobley DL, Gilson MK. The SAMPL4 Host–guest Blind Prediction Challenge: An Overview. J Comput Aided Mol Des. 2014 Mar; 28(4):305–317. doi: 10.1007/s10822-014-9735-1.

[13] **Mobley DL**, Liu S, Lim NM, Wymer KL, Perryman AL, Forli S, Deng N, Su J, Branson K, Olson AJ. Blind Prediction of HIV Integrase Binding from the SAMPL4 Challenge. J Comput Aided Mol Des. 2014 Mar; 28(4):327–345. doi: 10.1007/s10822-014-9723-5.

[14] **Yin J**, Henriksen NM, Slochower DR, Shirts MR, Chiu MW, Mobley DL, Gilson MK. Overview of the SAMPL5 Host–guest Challenge: Are We Doing Better? J Comput Aided Mol Des. 2017; 31(1):1–19. doi: 10.1007/s10822-016-9974-4.

[15] **Bannan CC**, Burley KH, Chiu M, Shirts MR, Gilson MK, Mobley DL. Blind Prediction of Cyclohexane–water Distribution Coefficients from the SAMPL5 Challenge. J Comput Aided Mol Des. 2016 Sep; 30(11):1–18. doi: 10.1007/s10822-016-9954-8.

[16] **Bannan CC**, Burley KH, Chiu M, Shirts MR, Gilson MK, Mobley DL. Blind prediction of cyclohexane–water distribution coefficients from the SAMPL5 challenge. Journal of Computer-Aided Molecular Design. 2016 Nov; 30(11):927–944. http://link.springer.com/10.1007/s10822-016-9954-8, doi: 10.1007/s10822-016-9954-8.

[17] **Rustenburg AS**, Dancer J, Lin B, Feng JA, Ortwine DF, Mobley DL, Chodera JD. Measuring experimental cyclohexane-water distribution coefficients for the SAMPL5 challenge. Journal of Computer-Aided Molecular Design. 2016 Nov; 30(11):945–958. http://link.springer.com/10.1007/s10822-016-9971-7, doi: 10.1007/s10822-016-9971-7.

[18] **Pickard FC**, König G, Tofoleanu F, Lee J, Simmonett AC, Shao Y, Ponder JW, Brooks BR. Blind prediction of distribution in the SAMPL5 challenge with QM based protomer and pK a corrections. Journal of Computer-Aided Molecular Design. 2016 Nov; 30(11):1087–1100. http://link.springer.com/10.1007/s10822-016-9955-7, doi: 10.1007/s10822-016-9955-7.

[19] **Bodner GM**. Assigning the pKa's of polyprotic acids. J Chem Educ. 1986; 63(3):246.

[20] **Darvey IG**. The assignment of pKa values to functional groups in amino acids. Wiley Online Library; 1995.

[21] **Bezençon J**, Wittwer MB, Cutting B, Smieško M, Wagner B, Kansy M, Ernst B. pKa determination by 1H NMR spectroscopy – An old methodology revisited. Journal of Pharmaceutical and Biomedical Analysis. 2014 May; 93:147–155. http://linkinghub.elsevier.com/retrieve/pii/S0731708513005992, doi: 10.1016/j.jpba.2013.12.014.

[22] **Elson EL**, Edsall JT. Raman spectra and sulfhydryl ionization constants of thioglycolic acid and cysteine. Biochemistry. 1962; 1(1):1–7.

[23] **Elbagerma MA**, Edwards HGM, Azimi G, Scowen IJ. Raman spectroscopic determination of the acidity constants of salicylaldoxime in aqueous solution. Journal of Raman Spectroscopy. 2011 Mar; 42(3):505–511. http://doi.wiley.com/10.1002/jrs.2716, doi: 10.1002/jrs.2716.

[24] **Sober HA**, Company CR. Handbook of Biochemistry: Selected Data for Molecular Biology. Handbook of Biochemistry: Selected Data for Molecular Biology, Chemical Rubber Company; 1970. https://books.google.com/books?id=16QRAQAAMAAJ.

[25] **Benesch RE**, Benesch R. The Acid Strength of the -SH Group in Cysteine and Related Compounds. Journal of the American Chemical Society. 1955; 77(22):5877–5881. https://doi.org/10.1021/ja01627a030, doi: 10.1021/ja01627a030.

[26] **Rupp M**, Korner R, V Tetko I. Predicting the pKa of small molecules. Combinatorial chemistry & high throughput screening. 2011; 14(5):307–327.

[27] **Marosi A**, Kovács Z, Béni S, Kökösi J, Noszál B. Triprotic acid–base microequilibria and pharmacokinetic sequelae of cetirizine. European Journal of Pharmaceutical Sciences. 2009 Jun; 37(3-4):321–328. http://linkinghub.elsevier.com/retrieve/pii/S0928098709000773, doi: 10.1016/j.ejps.2009.03.001.

[28] **Tam KY**, Takács-Novák K. Multi-wavelength spectrophotometric determination of acid dissociation constants: a validation study. Analytica chimica acta. 2001; 434(1):157–167.

[29] **Allen RI**, Box KJ, Comer JEA, Peake C, Tam KY. Multiwavelength spectrophotometric determination of acid dissociation constants of ionizable drugs. Journal of pharmaceutical and biomedical analysis. 1998; 17(4):699–712.

[30] **Comer JEA**, Manallack D. Ionization Constants and Ionization Profiles. In: *Reference Module in Chemistry, Molecular Sciences and Chemical Engineering* Elsevier; 2014.http://linkinghub.elsevier.com/retrieve/pii/B9780124095472112338, doi: 10.1016/B978-0-12-409547-2.11233-8.

[31] **Avdeef A**, Box KJ, Comer JEA, Gilges M, Hadley M, Hibbert C, Patterson W, Tam KY. PH-metric logP 11. pK a determination of water-insoluble drugs in organic solvent–water mixtures. Journal of pharmaceutical and biomedical analysis. 1999; 20(4):631–641.

[32] **Cabot JM**, Fuguet E, Rosés M, Smejkal P, Breadmore MC. Novel Instrument for Automated pK_a Determination by Internal Standard Capillary Electrophoresis. Analytical Chemistry. 2015 Jun; 87(12):6165–6172. http://pubs.acs.org/doi/10.1021/acs.analchem.5b00845, doi: 10.1021/acs.analchem.5b00845.

[33] **Wan H**, Holmén A, N\a ag\a ard M, Lindberg W. Rapid screening of pKa values of pharmaceuticals by pressure-assisted capillary electrophoresis combined with short-end injection. Journal of Chromatography A. 2002; 979(1-2):369–377.

[34] **Reijenga J**, van Hoof A, van Loon A, Teunissen B. Development of Methods for the Determination of pK_a Values. Analytical Chemistry Insights. 2013 Jan; 8:ACI.S12304. http://journals.sagepub.com/doi/10.4137/ACI.S12304, doi: 10.4137/ACI.S12304.

[35] **Sterling T**, Irwin JJ. ZINC 15 – Ligand Discovery for Everyone. Journal of Chemical Information and Modeling. 2015 Nov; 55(11):2324–2337. http://pubs.acs.org/doi/10.1021/acs.jcim.5b00559, doi: 10.1021/acs.jcim.5b00559.

[36] **Baell JB**, Holloway GA. New Substructure Filters for Removal of Pan Assay Interference Compounds (PAINS) from Screening Libraries and for Their Exclusion in Bioassays. Journal of Medicinal Chemistry. 2010 Apr; 53(7):2719–2740. http://pubs.acs.org/doi/abs/10.1021/jm901137j, doi: 10.1021/jm901137j.

[37] **Saubern S**, Guha R, Baell JB. KNIME Workflow to Assess PAINS Filters in SMARTS Format. Comparison of RDKit and Indigo Cheminformatics Libraries. Molecular Informatics. 2011 Oct; 30(10):847–850. http://doi.wiley.com/10.1002/minf.201100076, doi: 10.1002/minf.201100076.

[38] eMolecules Database Free Version;. Accessed: 2017-06-01. https://www.emolecules.com/info/products-data-downloads.html.

[39] OEChem Toolkit 2017.Feb.1;. OpenEye Scientific Software, Santa Fe, NM. http://www.eyesopen.com.

[40] **Shelley JC**, Cholleti A, Frye LL, Greenwood JR, Timlin MR, Uchimaya M. Epik: a software program for pK_a prediction and protonation state generation for drug-like molecules. Journal of Computer-Aided Molecular Design. 2007 Dec; 21(12):681–691. http://link.springer.com/10.1007/s10822-007-9133-z, doi: 10.1007/s10822-007-9133-z.

[41] Schrödinger Release 2016-4: Epik Version 3.8;. Schrödinger, LLC, New York, NY, 2016.

[42] OEMolProp Toolkit 2017.Feb.1;. OpenEye Scientific Software, Santa Fe, NM. http://www.eyesopen.com.

[43] **Wishart DS**. DrugBank: a comprehensive resource for in silico drug discovery and exploration. Nucleic Acids Research. 2006 Jan; 34(90001):D668–D672. https://academic.oup.com/nar/article-lookup/doi/10.1093/nar/gkj067, doi: 10.1093/nar/gkj067.

[44] **Pence HE**, Williams A. ChemSpider: An Online Chemical Information Resource. Journal of Chemical Education. 2010 Nov; 87(11):1123–1124. http://pubs.acs.org/doi/abs/10.1021/ed100697w, doi: 10.1021/ed100697w.

[45] NCI Open Database, August 2006 Release;. https://cactus.nci.nih.gov/download/nci/.

[46] Enhanced NCI Database Browser 2.2;. https://cactus.nci.nih.gov/ncidb2.2/.

[47] **Kim S**, Thiessen PA, Bolton EE, Chen J, Fu G, Gindulyte A, Han L, He J, He S, Shoemaker BA, Wang J, Yu B, Zhang J, Bryant SH. PubChem Substance and Compound databases. Nucleic Acids Research. 2016 Jan; 44(D1):D1202–D1213. https://academic.oup.com/nar/article-lookup/doi/10.1093/nar/gkv951, doi: 10.1093/nar/gkv951.

[48] NCI/CADD Chemical Identifier Resolver;. https://cactus.nci.nih.gov/chemical/structure.

[49] **Bemis GW**, Murcko MA. The properties of known drugs. 1. Molecular frameworks. Journal of medicinal chemistry. 1996; 39(15):2887–2893.

[50] OEMedChem Toolkit 2017.Feb.1;. OpenEye Scientific Software, Santa Fe, NM. http://www.eyesopen.com.

[51] Sirius T3 User Manual, v1.1. Sirius Analytical Instruments Ltd, East Sussex, UK; 2008.

[52] **Avdeef A**, Comer JEA, Thomson SJ. pH-Metric log P. 3. Glass electrode calibration in methanol-water, applied to pKa determination of water-insoluble substances. Analytical Chemistry. 1993; 65(1):42–49. https://doi.org/10.1021/ac00049a010, doi: 10.1021/ac00049a010.

[53] **Takács-Novák K**, Box KJ, Avdeef A. Potentiometric pKa determination of water-insoluble compounds: validation study in methanol/water mixtures. International Journal of Pharmaceutics. 1997; 151(2):235 – 248. http://www.sciencedirect.com/science/article/pii/S0378517397049077, doi: https://doi.org/10.1016/S0378-5173(97)04907-7.

[54] **Szakacs Z**, Beni S, Varga Z, Orfi L, Keri G, Noszal B. Acid-Base Profiling of Imatinib (Gleevec) and Its Fragments. Journal of Medicinal Chemistry. 2005; 48(1):249–255. https://doi.org/10.1021/jm049546c, doi: 10.1021/jm049546c, pMID: 15634018.

[55] **Szakacs Z**, Kraszni M, Noszal B. Determination of microscopic acid?base parameters from NMR?pH titrations. Analytical and Bioanalytical Chemistry. 2004 Mar; 378(6):1428–1448. http://link.springer.com/10.1007/s00216-003-2390-3, doi: 10.1007/s00216-003-2390-3.

[56] **Dozol H**, Blum-Held C, Guédat P, Maechling C, Lanners S, Schlewer G, Spiess B. Inframolecular acid–base studies of the tris and tetrakis myo-inositol phosphates including the 1, 2, 3-trisphosphate motif. Journal of molecular structure. 2002; 643(1-3):171–181.

[57] OEDepict Toolkit 2017.Feb.1;. OpenEye Scientific Software, Santa Fe, NM. http://www.eyesopen.com.

[58] **Fraczkiewicz R**. In Silico Prediction of Ionization. In: *Reference Module in Chemistry, Molecular Sciences and Chemical Engineering* Elsevier; 2013.http://linkinghub.elsevier.com/retrieve/pii/B978012409547202610X, doi: 10.1016/B978-0-12-409547-2.02610-X.